

# Hybrid Beamforming NOMA for mmWave Communications

Mojtaba Ahmadi Almasi, Mojtaba Vaezi, Hani Mehrpouyan

## Abstract

This paper studies hybrid beamforming (HB)-based non-orthogonal multiple access (NOMA) in multiuser millimeter wave (mmWave) communications. HB offers power-efficient and low-complexity precoding for downlink multiuser mmWave systems which increases multiplexing gain and spectral efficiency of the system. Applying NOMA to HB-based systems, called HB-NOMA, can scale the number of users while offering a high spectral efficiency. However, an imperfect correlation between the effective channels of users in each NOMA cluster seriously degrades the achievable rate of HB-NOMA. In this paper, first a sum-rate maximization problem is formulated for HB-NOMA, and an algorithm is proposed to solve it effectively. It is then shown that the relationship between the effective channels of the users in each NOMA cluster can be approximated by a correlation factor. Next, the effect of imperfect correlation is analyzed, and a lower bound on the achievable rate of the users is derived for both perfect and imperfect correlation. Finally, the rate gap resulting from an imperfect correlation is evaluated and a tight upper bound is derived for that. Simulation results show that low correlation degrades the achievable rate of users. The lower bounds are tight in the large dimensional regime and in single-path channels.

## Index Terms

Hybrid beamforming, NOMA, sum-rate, perfect correlation, imperfect correlation, optimization.

This project was supported in part by the NSF ERAS under Grant 1642865.

M. A. Almasi and H. Mehrpouyan are with the Department of Electrical and Computer Engineering, Boise State University, Boise, ID 83725, USA (e-mail: {mojtabaahmadalm, hanimehrpouyan}@boisestate.edu).

M. Vaezi is with the Department of Electrical and Computer Engineering, Villanova University, Villanova, PA 19085, USA. He is also a Visiting Research Collaborator at Princeton University (e-mail: mvaezi@princeton.edu).

## I. INTRODUCTION

*Millimeter wave* (mmWave) communications has emerged as one of the key solutions for fifth-generation (5G) wireless networks. The existence of large unused spectrum at mmWave band (30-300 GHz) offers the potential for significant throughput gains. Shorter wavelengths of the mmWave band, on the other hand, allow for the deployment of large numbers of antenna elements at both the base station (BS) and mobile users, which, in turn, enables mmWave systems to support higher degrees of *multiplexing* gain in the multi-input multi-output (MIMO) and *multiuser MIMO* systems [1]–[3]. To this end, the BS needs to apply some form of *beamforming*. This beamforming can be done in the baseband, radio frequency (RF), or a combination of the two. While *baseband beamforming* (fully-digital) offers a better control over the entries of the precoding matrix, it is unlikely with current semiconductor technologies due to the high cost and power consumption.

*Analog beamforming* is an alternative to the baseband beamforming which controls the phase of the signal transmitted at each antenna using analog phase shifters implemented in the RF domain. Fully-analog beamforming which uses one *RF chain*, see, e.g. [4], can, however, support only one data stream. In order to transmit multiple streams, by exploiting several RF chains, *hybrid analog/digital beamforming* mmWave systems are designed [5], [6]. In [7] and [8], the concept of beamspace MIMO is introduced where several RF chains are connected to a lens antenna array via switches. Recently, multi-beam lens-based reconfigurable antenna MIMO systems have been proposed to overcome severe path loss and shadowing in mmWave frequencies [9], [10]. In the aforementioned systems, each beam is considered to serve only one user. The works in [11] and [12] show that exploiting hybrid beamforming in multiuser systems achieves a higher spectral efficiency. Also, [13] enhances the spectral efficiency by supporting several users through multi-beam reconfigurable antenna. Nevertheless, the number of served users are far less than the number of users envisioned for 5G networks.

*Non-orthogonal multiple access* (NOMA) is another enabling technique for 5G networks that augments the number of users and spectral efficiency in multiuser scenarios [14]–[21]. Unlike orthogonal multiple access (OMA) techniques, such as time division multiple access (TDMA), frequency division multiple access (FDMA), and code division multiple access (CDMA) which can support only one user per time, frequency, or code, respectively, NOMA can support multiple users in the same time/frequency/code. NOMA can be realized in the code, power, or other domains [22]. In the power domain, NOMA employs *superposition coding* at the transmitter. This technique exploits the channel gain difference between users

to multiplex their signal. Subsequently, *successive interference cancellation* (SIC) is applied at the receiver such that the user with better channel first decodes the signal of the user with worse channel and then subtracts it from the received signal to decode its own signal [14]–[23].

Transmission in mmWave band suffers from high path loss and thus users in different locations may experience very different channel gains. This implies that mmWave band better suits power domain NOMA which offers a larger spectral efficiency when the channel gain difference between the users is high. Integration of NOMA into mmWave systems, which allows multiple users to share the same beam, has been studied in [24]–[29]. In [24], a random beamforming technique is designed for mmWave NOMA systems where the BS randomly radiates a directional beam toward paired users. In [25], it is shown that mismatch between the users' channel vector and finite resolution analog beamforming<sup>1</sup> simplifies utilizing NOMA in MIMO mmWave systems. In [26], a combination of beamspace MIMO and NOMA is proposed to ensure that the number of served users is not limited to the number of RF chains. In [27], NOMA is studied for hybrid MIMO mmWave systems, where a power allocation algorithm has been provided in order to maximize energy efficiency. In all aforementioned works, NOMA is combined with mmWave systems assuming only baseband precoders/combiners. The works in [28] and [29] have recently studied *hybrid beamforming* (HB) in NOMA systems. In [28], designing beamforming vectors and allocating power for two users has been studied. In [29], it is demonstrated that due to the utilization of HB, the digital precoder of the BS is not perfectly aligned with the user's effective channel. Based on the imperfect aligned beams, a power allocation algorithm that maximizes the sum-rate has been proposed [29]. However, these works fail to study the effect of imperfect beamforming on the sum-rate. In our prior work [30] the concept of hybrid beamforming NOMA (HB-NOMA) has been introduced. Initial studies show that the achievable rate of each user widely depends on the correlation between the effective channels of the NOMA users in each cluster [30].

In this paper, we investigate the impact of imperfect correlation between effective channels on the sum-rate performance of HB-NOMA systems. We first evaluate the sum-rate expression for perfect correlation between the users. We next extend the evaluations to the imperfect correlation case. Finally, we derive the rate loss due to the imperfect correlation. We consider a single-cell scenario in which a BS is equipped with an HB system transmits several streams through the formed beams and each beam is allowed to be shared with multiple users inside a cluster (see Fig. 1). Unlike digital beamformers, the HB precoders are

<sup>1</sup>Finite resolution analog beamforming is due to the use of a finite number of phase shifters in the analog beamformer.

not able to perfectly align a beam toward all users due to the finite resolution of analog beamformers. Hence, the evaluation of achievable rates for HB-NOMA under the non-ideal beam alignment is necessary. We model this misalignment with a correlation factor. The factor takes a value between 0 and 1 where 1 shows the perfect correlation and other values show imperfect correlation. Since we aim to study the effect of misalignment, other parameters of the system will be considered ideal. The contribution of this paper is summarized as follows.

- 1) Since we aim to evaluate the impact of the correlation between the effective channels on HB-NOMA systems, a sum-rate expression is formulated. Then, an algorithm is proposed to maximize the system sum-rate subject to a total power constraint, in three steps. The first step designs the analog precoder/combiner; the second step obtains the digital precoder; and, the last step introduces a suboptimal power allocation procedure.
- 2) As the maximized sum-rate directly depends on the effective channels of users, we study the impact of correlation between the effective channels for the perfect correlation and imperfect correlation. The perfect correlation, which is due to perfect effective channel alignment among all users inside a cluster, does not impose extra interference on the achievable rate. In the case that the correlation is perfect, a lower bound is derived for the achievable rate of an HB-NOMA user. The bound indicates that the interference is due to using NOMA and hybrid beamforming. However, the analysis shows that, with a perfect correlation, HB-NOMA can achieve a rate which is close to the digital beamforming.
- 3) We study the achievable rate of each user for misaligned effective channels. To achieve this goal, a misalignment is modeled by an imperfect correlation. The model shows that a higher misalignment leads to a lesser correlation. Considering the derived model, we extract a lower bound for the achievable rate. According to the bound, three terms, i.e., intra-cluster interference, inter-cluster interference, and noise, constrain the achievable rate. Unfortunately, these terms directly or indirectly are associated with the correlation factor, such that a low correlation reduces the intra-cluster interference, increases the inter-cluster interference and noise. Hence, under an imperfect correlation, the rate could be considerably smaller.
- 4) We also evaluate the data-rate loss due to the imperfect correlation and derive an upper bound for the gap between the rate of the users with perfect correlation and imperfect correlation. The analytical result demonstrates that the gap depends on the correlation factor, intra-cluster interference, inter-

cluster interference, and the design of the baseband precoder.

The paper is organized as follows: Section II presents the system model for the proposed HB-NOMA system. In Section III, first we derive an expression for the sum-rate for the proposed HB-NOMA system. Then, an algorithm is proposed that maximizes the sum-rate. Section IV derives two lower bounds on user rates with perfect and imperfect correlation channels. An upper bound for user rate is derived in Section V. In Section VI, we present simulation results investigating the performance of the system. Section VII concludes the paper.

**Notations:** Hereafter,  $j = \sqrt{-1}$ , small letters, bold letters and bold capital letters will designate scalars, vectors, and matrices, respectively. Superscripts  $(\cdot)^T$  and  $(\cdot)^\dagger$  denote the transpose and transpose-conjugate operators, respectively. Further,  $|\cdot|$ , and  $\|\cdot\|^2$  denote the absolute value, and norm-2 of  $(\cdot)$ , respectively. Indeed,  $\|\cdot\|_F^2$  denotes the Frobenius norm of matrix  $(\cdot)$ . Finally,  $\mathbb{E}[\cdot]$  denotes the expected value of  $(\cdot)$ .

## II. SYSTEM MODEL

This section describes an HB-NOMA system. Toward this goal, first we review a simple NOMA scheme.

### A. Overview of NOMA

Consider the downlink transmission of a single cell communication system with a BS serving multiple users. For the purpose of illustration, assume the number of users is restricted to two. Let the BS allocate power  $P_i$  ( $i = 1, 2$ ) to transmit signal  $s_i$  to the  $i$ th user denoted by  $U_i$ , where  $\mathbb{E}[|s_i|^2] = 1$  and sum of  $P_i$ s equals to  $P$ . The transmitted signal in NOMA is a superposition of  $s_1$  and  $s_2$ , scaled with their corresponding powers, i.e.,

$$x = \sqrt{P_1}s_1 + \sqrt{P_2}s_2. \quad (1)$$

Then, the received signal at  $U_i$ , for  $i = 1, 2$ , is given by

$$y_i = h_i x + n_i = h_i (\sqrt{P_1}s_1 + \sqrt{P_2}s_2) + n_i, \quad (2)$$

where  $h_i$  is the complex channel gain between the BS and  $U_i$ , and  $n_i$  denotes the additive white Gaussian noise with power 1. At the receiver, the stronger user performs SIC to decode the desired signal. The optimal decoding order depends on the channel gain. Without loss of generality, let us assume that  $U_1$  has strong channel gain, i.e.,  $|h_1|^2 \geq |h_2|^2$ , which gives  $P_1 \leq P_2$ .

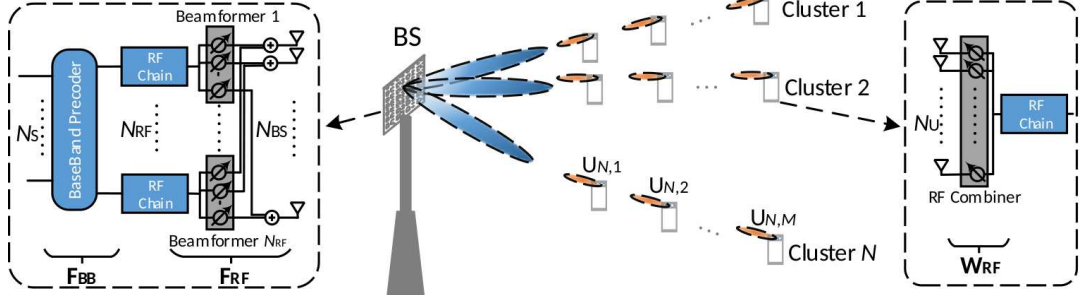


Fig. 1: HB-NOMA with one BS and  $NM$  users grouped into  $N$  clusters each with  $M$  NOMA users.  $N_S$ ,  $N_{RF}$ ,  $N_{BS}$ , and  $N_U$  are the numbers of multiplexed streams, RF chains, BS antennas, and user antennas, respectively.

Then, the achievable rate for  $U_i$  ( $i = 1, 2$ ) is given as

$$\begin{aligned} R_1 &= \log_2 \left( 1 + P_1 |h_1|^2 \right), \\ R_2 &= \log_2 \left( 1 + \frac{P_2 |h_2|^2}{P_1 |h_2|^2 + 1} \right), \end{aligned} \quad (3)$$

and the sum-rate of this NOMA system becomes  $R = R_1 + R_2$ .

### B. System Model for HB-NOMA

Now, we consider a narrow band mmWave downlink system composed of a BS and multiple users as shown in Fig. 1. The BS is equipped with  $N_{RF}$  chains and  $N_{BS}$  antennas whereas each user has one RF chain and  $N_U$  antennas. Further, we assume that the BS communicates with each user via only one stream. In traditional multiuser systems based on the hybrid beamforming the maximum number of users that can be simultaneously served by the BS equals the number of BS RF chains [12].

In order to establish a better connectivity in dense areas and further improve the sum-rate, this paper utilizes NOMA in hybrid beamforming multiuser systems where each beam is allowed to serve more than one user. The transmitter sends  $N_S$  streams at the same time toward  $M$  users which are grouped into  $N \leq N_{RF}$  clusters. Without loss of generality, we assume  $N_S = N$ . Hence,  $MN \gg N_{RF}$ ; i.e., the proposed HB-NOMA system can simultaneously serve  $MN$  users which is much larger than the number of RF chains.

On the downlink, the hybrid beamforming is done in two stages. In the first stage, the transmitter applies an  $N \times N$  baseband precoder  $\mathbf{F}_{BB}$  using its  $N_{RF}$  RF chains. This stage then is followed by an  $N_{BS} \times N$  RF precoder  $\mathbf{F}_{RF}$  using analog phase shifters. Thus, the transmit signal vector is given by

$$\mathbf{x} = \mathbf{F}_{RF} \mathbf{F}_{BB} \mathbf{s}, \quad (4)$$

where  $\mathbf{s} = [s_1, s_2, \dots, s_N]^T$  denotes the information signal vector such that  $\mathbb{E}[\mathbf{s}\mathbf{s}^\dagger] = \frac{1}{N}\mathbf{I}$  in which  $\mathbf{I}$  is an  $N \times N$  identity matrix. Each  $s_n = \sum_{m=1}^M \sqrt{P_{n,m}}s_{n,m}$  is the superposition coded signal performed by NOMA with  $P_{n,m}$  and  $s_{n,m}$  being transmit power and transmit information signal for the  $\mathbf{U}_m$  in the  $n$ th cluster. Hereafter,  $\mathbf{U}_{n,m}$  denotes the  $m$ th user in the  $n$ th cluster. Since  $\mathbf{F}_{\text{RF}}$  is implemented by using analog phase shifters it is assumed that all elements of  $\mathbf{F}_{\text{RF}}$  have an equal norm, i.e.,  $|\mathbf{F}_{\text{RF}}|_F^2 = N_{\text{BS}}^{-1}$ . Also, the total power of the hybrid transmitter is constrained to  $\|\mathbf{F}_{\text{RF}}\mathbf{F}_{\text{BB}}\|_F^2 = N$ . The received signal at  $\mathbf{U}_{n,m}$  is given by

$$\mathbf{r}_{n,m} = \mathbf{H}_{n,m}\mathbf{F}_{\text{RF}}\mathbf{F}_{\text{BB}}\mathbf{s} + \mathbf{n}_{n,m}, \quad (5)$$

where  $\mathbf{H}_{n,m}$  of size  $N_{\text{U}} \times N_{\text{BS}}$  denotes the mmWave channel between the BS and  $\mathbf{U}_{n,m}$  such that  $\mathbb{E}[\|\mathbf{H}_{n,m}\|_F^2] = N_{\text{BS}}N_{\text{U}}$ .  $\mathbf{n}_{n,m} \sim \mathcal{CN}(\mathbf{0}, \mathbf{I})$  is the additive white Gaussian noise vector of size  $N_{\text{U}} \times 1$ . At  $\mathbf{U}_{n,m}$ , the RF combiner is used to process the received vector as

$$\begin{aligned} y_{n,m} = & \underbrace{\mathbf{w}_{n,m}^\dagger \mathbf{H}_{n,m} \mathbf{F}_{\text{RF}} \mathbf{f}_{\text{BB}}^n \sqrt{P_{n,m}} s_{n,m}}_{\text{desired signal}} + \underbrace{\mathbf{w}_{n,m}^\dagger \mathbf{H}_{n,m} \mathbf{F}_{\text{RF}} \mathbf{f}_{\text{BB}}^n \sum_{k \neq m}^M \sqrt{P_{n,k}} s_{n,k}}_{\text{intra-cluster interference}} \\ & + \underbrace{\mathbf{w}_{n,m}^\dagger \mathbf{H}_{n,m} \sum_{\ell=1, \ell \neq n}^N \mathbf{F}_{\text{RF}} \mathbf{f}_{\text{BB}}^\ell \sum_{q=1}^M \sqrt{P_{\ell,q}} s_{\ell,q}}_{\text{inter-cluster interference}} + \underbrace{\mathbf{w}_{n,m}^\dagger \mathbf{n}_{n,m}}_{\text{noise}}, \end{aligned} \quad (6)$$

where  $\mathbf{w}_{n,m} \in \mathbb{C}^{N_{\text{U}} \times 1}$  denotes the combiner at  $\mathbf{U}_{n,m}$ . After combining, each user decodes the intended signal by using SIC. More details on SIC will be provided in Section III.

In mmWave communications, the single-path channel between the BS and  $\mathbf{U}_{n,m}$  can be expressed as

$$\mathbf{H}_{n,m} = \sqrt{N_{\text{BS}}N_{\text{U}}} \beta_{n,m} \mathbf{a}_{\text{U}}(\vartheta_{n,m}) \mathbf{a}_{\text{BS}}^\dagger(\varphi_{n,m}), \quad (7)$$

where  $\beta_{n,m} = g_{n,m} d_{n,m}^{-\frac{\nu}{2}}$  with  $g_{n,m}$  is the complex gain with zero-mean and unit-variance,  $d_{n,m}$  is the distance between the BS and  $\mathbf{U}_{n,m}$ , and  $\nu$  is the path loss factor. Also,  $\mathbf{a}_{\text{BS}}(\varphi_{n,m})$  and  $\mathbf{a}_{\text{U}}(\vartheta_{n,m})$  are the antenna array response vector of the BS and  $\mathbf{U}_{n,m}$  where  $\vartheta_{n,m}$  and  $\varphi_{n,m} \in [-1, 1]$  are related to the angle of arrival (AoA)  $\vartheta \in [-\frac{\pi}{2}, \frac{\pi}{2}]$  and angle of departure (AoD)  $\varphi \in [-\frac{\pi}{2}, \frac{\pi}{2}]$  as  $\vartheta_{n,m} = \frac{2d\sin(\vartheta)}{\lambda}$  and  $\varphi_{n,m} = \frac{2d\sin(\varphi)}{\lambda}$ , respectively [6], [12]. Note that  $d$  denotes the antenna spacing and  $\lambda$  denotes the wavelength of the propagation.

In particular, for a uniform linear array (ULA),  $\mathbf{a}_{\text{BS}}(\varphi_{n,m})$  is given by

$$\mathbf{a}_{\text{BS}}(\varphi_{n,m}) = \frac{1}{\sqrt{N_{\text{BS}}}} \left[ 1, e^{-j\pi\varphi_{n,m}}, \dots, e^{-j\pi(N_{\text{BS}}-1)\varphi_{n,m}} \right]^T. \quad (8)$$

The antenna array response vector for  $\mathbf{a}_{\text{U}}(\vartheta_{n,m})$  can be written in a similar fashion [6], [12].

In order to focus on the effect of digital/analog precoding on the sum-rate expression, the following ideal assumptions are considered.<sup>2</sup>

- Full CSI of each user,  $\mathbf{H}_{n,m}$ ,  $m = 1, 2, \dots, M$  and  $n = 1, 2, \dots, N$ , is available at every user. This assumption is ideal since the channel estimation error is not considered.
- The BS and all users steer the beams with continuous angles. That is, the quantization error is neglected for  $\mathbf{F}_{\text{RF}}$  and  $\mathbf{w}_{n,m}$ ,  $m = 1, 2, \dots, M$  and  $n = 1, 2, \dots, N$ .
- The first user of each cluster feeds perfect effective channel back to the BS which means infinite-resolution codebooks are used. In practical scenarios, the receiver employs finite-size predefined codebooks to quantize its effect channel, then feeds it back to the BS [31], [32].
- The BS knows all users' channel gain  $|\beta_{n,m}|$ ,  $m = 1, 2, \dots, M$  and  $n = 1, 2, \dots, N$ .
- Each user is capable of performing error-free SIC.

### III. SUM-RATE FOR HB-NOMA

The goal of this work is to study the impact of utilization of NOMA in hybrid beamforming systems. In particular, we study the effect of simultaneously designing hybrid precoders and analog combiners for clustered users on the performance of the achievable rate. Here, we first derive a sum-rate expression for HB-NOMA. Then, an algorithm is proposed to maximize the sum-rate.

#### A. Sum-Rate Formulation

In (6) after applying superposition coding at the transmitter, each user experiences two types of interference. Intra-cluster interference which is due to other users within the cluster and inter-cluster interference which is due to users within other clusters. Suppressing the intra-cluster interference directly depends on efficient power allocation and deploying SIC. At the receiver side, each user performs SIC to decode the desired signal. To do this, first the signal of the strongest users is decoded then subtracted from the received signal. The process continues until the intended user decodes its own signal. The remaining

<sup>2</sup>The non-ideal assumptions will be studied in the authors' future works.

is intra-cluster interference which is buried in the signal. Here, we assume that each user can perfectly perform SIC decoding. To mitigate the inter-cluster interference, the transmitter needs to design a proper beamforming matrix. In this paper, we adopt zero-forcing beamforming (ZFBF) which makes a balance between implementation complexity and performance [33], [34].

We will evaluate the sum-rate for the proposed HB-NOMA. The rate for  $U_{n,m}$  is expressed as

$$R_{n,m} = \log_2 \left( 1 + \frac{P_{n,m} |\mathbf{w}_{n,m}^\dagger \mathbf{H}_{n,m} \mathbf{F}_{\text{RF}} \mathbf{f}_{\text{BB}}^n|^2}{I_{\text{intra}}^{n,m} + I_{\text{inter}}^{n,m} + 1} \right), \quad (9)$$

where  $I_{\text{intra}}^{n,m}$  is given by

$$I_{\text{intra}}^{n,m} = \sum_{k=1}^{m-1} P_{n,k} |\mathbf{w}_{n,m}^\dagger \mathbf{H}_{n,m} \mathbf{F}_{\text{RF}} \mathbf{f}_{\text{BB}}^n|^2, \quad (10)$$

denotes the intra-cluster interference after SIC. Notice that to get (10), without loss of generality, the first user in each cluster is assumed to have the highest channel gain which is allocated the lowest power and the  $M$ th user has the lowest channel gain which is allocated the highest power. According to NOMA,  $U_{n,m}$  decodes the intended signal of  $U_{n,k'}$ , i.e.,  $s_{n,k'}$ , for  $k' = m+1, m+2, \dots, M$  and subtracts it from the received signal  $y_{n,m}$ . However, NOMA treats the intended signal of  $U_{n,k}$  for  $k = 1, 2, \dots, m-1$  as intra-cluster interference. Also,  $I_{\text{inter}}^{n,m}$  is defined as

$$I_{\text{inter}}^{n,m} = \sum_{\ell=1, \ell \neq n}^N \sum_{q=1}^M P_{\ell,q} |\mathbf{w}_{n,m}^\dagger \mathbf{H}_{n,m} \mathbf{F}_{\text{RF}} \mathbf{f}_{\text{BB}}^\ell|^2, \quad (11)$$

denotes the inter-cluster interference.

To improve the sum-rate performance, hybrid precoder  $\mathbf{F}_{\text{RF}}$ , and  $\mathbf{F}_{\text{BB}}$ , combiner  $\mathbf{w}_{n,m}$  and transmit power  $P_{n,m}$  for  $m = 1, 2, \dots, M$  and  $n = 1, 2, \dots, N$  should be found from

$$\mathbf{F}_{\text{RF}}, \mathbf{F}_{\text{BB}}, \mathbf{w}_{n,m}, P_{n,m} \quad \sum_{n=1}^N \sum_{m=1}^M R_{n,m} \quad (12a)$$

$$\text{subject to} \quad |(\mathbf{F}_{\text{RF}})_{n,m}|^2 = N_{\text{BS}}^{-1}, \quad (12b)$$

$$\|\mathbf{F}_{\text{RF}} \mathbf{F}_{\text{BB}}\|_F^2 = N, \quad (12c)$$

$$|\mathbf{w}_{n,m}|^2 = N_{\text{U}}^{-1}, \quad (12d)$$

$$\sum_{n=1}^N \sum_{m=1}^M P_{n,m} \leq P, \quad (12e)$$

$$P_{n,m} > 0, \quad (12f)$$

where  $P$  equals to the total transmit power. In the above optimization problem, the constraints (12b) and (12d) ensure that all elements of  $\mathbf{F}_{\text{RF}}$  and  $\mathbf{w}_n$  have an equal norm. Further, the constrain (12c) ensures that the total power of the hybrid transmitter is limited to  $N$ . The constrain (12e) guarantees that the total transmit power is limited to  $P$ . The constrain (12f) ensures that the allocated power to  $\mathbf{U}_{n,m}$  is greater than zero. So, this user is always sent an intended signal.

### B. The Maximization Algorithm

The maximization problem in (12) is non-convex and finding the optimal solution is not trivial. Alternatively, we propose a suboptimal but effective algorithm in three steps as described below.

In the first step, the BS and  $\mathbf{U}_{n,m}$  solve the following problem

$$\begin{aligned} & \underset{\mathbf{w}_{n,m}, \mathbf{f}_{\text{RF}}^{n,m}}{\text{maximize}} \quad |\mathbf{w}_{n,m}^\dagger \mathbf{H}_{n,m} \mathbf{f}_{\text{RF}}^{n,m}| \\ & \text{subject to (12b) and (12d).} \end{aligned} \quad (13)$$

Since the channel  $\mathbf{H}_{n,m}$  has only one path, and given the continuous beamsteering capability assumption, in view of (7),

$$\mathbf{w}_{n,m} = \mathbf{a}_{\text{U}}(\vartheta_{n,m}), \quad (14)$$

and

$$\mathbf{f}_{\text{RF}}^{n,m} = \mathbf{a}_{\text{BS}}(\varphi_{n,m}), \quad (15)$$

are the optimal solutions. In order to design RF precoder, the BS selects the first user of each cluster. So, the RF precoder of the first user of the  $n$ th cluster makes the  $n$ th column of the RF precoding matrix, i.e.,  $\mathbf{f}_{\text{RF}}^{n,1}$  for  $n = 1, 2, \dots, N$ , gives the RF precoding matrix as

$$\mathbf{F}_{\text{RF}} = \left[ \mathbf{f}_{\text{RF}}^{1,1}, \mathbf{f}_{\text{RF}}^{2,1}, \dots, \mathbf{f}_{\text{RF}}^{N,1} \right]. \quad (16)$$

Here, the first user is selected based on the following criterion:

$$|\beta_{n,1}| \geq |\beta_{n,2}| \geq \dots \geq |\beta_{n,M}|, \quad \text{for } n = 1, 2, \dots, N, \quad (17)$$

where  $\beta_{n,m}$  is the gain factor defined in (7).

In the second step, the effective channel for  $U_{n,m}$  is expressed as

$$\begin{aligned}\bar{\mathbf{h}}_{n,m}^\dagger &= \mathbf{w}_{n,m}^\dagger \mathbf{H}_{n,m} \mathbf{F}_{\text{RF}} \\ &= \sqrt{N_{\text{BS}} N_{\text{U}}} \beta_{n,m} \mathbf{a}_{\text{BS}}^\dagger(\varphi_{n,m}) \mathbf{F}_{\text{RF}}.\end{aligned}\quad (18)$$

We write the effective channel matrix as

$$\bar{\mathbf{H}} = [\bar{\mathbf{h}}_{1,1}, \bar{\mathbf{h}}_{2,1}, \dots, \bar{\mathbf{h}}_{N,1}]^\dagger, \quad (19)$$

where  $\bar{\mathbf{h}}_{n,1}$  denotes the effective channel vector of  $U_{n,1}$ . The reason for this selection is that based on HB-NOMA the first user of each cluster has to decode other users' signal in that cluster. Thus, steering the beam toward the first user can lead to a reliable SIC. Hence, the RF precoder has to be designed based on (16) to reduce the intra-cluster interference. Also, the effective channel matrix (19) causes the inter-cluster interference on the first users to be completely removed. This subject is justified in the following.

Designing a proper digital precoder  $\mathbf{F}_{\text{BB}}$  remarkably reduces the inter-cluster interference. In brief, designing the baseband precoder becomes equivalent to solving

$$\underset{\{\mathbf{f}_{\text{BB}}^\ell\}_{\ell \neq n}}{\text{minimize}} I_{\text{inter}}^{n,m} \quad \text{subject to (12c).} \quad (20)$$

where  $I_{\text{inter}}^{n,m}$  is defined in (10). Finding an optimal minimum in (20) is challenging. Hence, we select a suboptimal solution, e.g., ZFBF scheme, to design  $\mathbf{F}_{\text{BB}}$ . Based on ZFBF the solution for (20) is obtained as

$$\mathbf{F}_{\text{BB}} = \bar{\mathbf{H}}^\dagger \left( \bar{\mathbf{H}} \bar{\mathbf{H}}^\dagger \right)^{-1} \Lambda, \quad (21)$$

where the diagonal elements of  $\Lambda$  are given by [12]

$$\Lambda_{n,n} = \sqrt{\frac{N_{\text{BS}} N_{\text{U}}}{(\mathbf{F}^{-1})_{n,n}}} |\beta_{n,1}|, \quad \text{for } n = 1, 2, \dots, N. \quad (22)$$

A deeper look at (21) indicates that inter-cluster interference on first users is zero, i.e.,  $\bar{\mathbf{h}}_{n,1}^\dagger \mathbf{f}_{\text{BB}}^\ell = 0$  for  $n = 1, 2, \dots, N$  and  $\ell \neq n$ . That is, inter-cluster interference is perfectly eliminated for the first user of each cluster. This completes our justification about the orienting the beams toward the first users and choosing their effective channel vector in designing  $\mathbf{F}_{\text{BB}}$ .

In the third step, the BS first reorders the users then allocates the power. The reordering process is done based on the effective channel vectors as

$$\|\bar{\mathbf{h}}_{n,1}\| \geq \|\bar{\mathbf{h}}_{n,2}\| \geq \cdots \geq \|\bar{\mathbf{h}}_{n,M}\|, \quad \text{for } n = 1, 2, \dots, N. \quad (23)$$

It is worth mentioning that in (17) we aimed to find the first users based on the large-scale gain. However, in HB-NOMA the power allocation is conducted based on order of the effective channel gains. While the first user in (17) is the same as the first user in (23), the order of the other users might change. Intuitively speaking, the users whose beam directions are close to the first user's beam would have a stronger effective channel compared to the users which have a better large-scale gain but do not have a close beam direction to the first user's beam.

The optimal power allocation in (12) is non-trivial and iterative procedures are needed to solve

$$\begin{aligned} & \underset{P_{n,m}}{\text{maximize}} \quad \sum_{n=1}^N \sum_{m=1}^M R_{n,m} \\ & \text{subject to (12e) and (12f).} \end{aligned} \quad (24)$$

Obtaining the optimal solution for (24) is very challenging. Hence, we propose a suboptimal solution. Our solution has two stages. First the BS divides its power equally between the clusters, i.e.,  $P_c = P/N$ . Then a fixed power allocation [17] is utilized for the users in each cluster respecting the constraint  $\sum_{m=1}^M P_{n,m} = P_c$  which completes the proposed algorithm. These three steps are summarized in Algorithm 1 on the next page.

A different interpretation for the optimization problem in (12) can be explained as follows. The problem aims to serve  $NM$  users by using only  $N_{\text{RF}}$  chains and the total power  $P$  in order to maximize the sum-rate given in (12a). To this end, first of all, the users are divided into  $N$  clusters. In this paper, we assume that the users are properly clustered. Since the effective channels of the first users are independent, they define an  $N$  dimensional space. The baseband beamforming matrix  $\mathbf{F}_{\text{BB}}$  aligns the effective channels of the first users to the  $N$  subspaces. Then, the effective channels of remaining  $M - 1$  users located in a cluster should be aligned as close as to that of the first user. Designing a proper effective channel for these users is beyond the scope of this paper and will consider in the authors' future work. Then, NOMA is exploited to serve  $M$  users in each cluster. Unfortunately, the effective channels of the  $M - 1$  users is not completely aligned toward the effective channels of the first user. This causes a portion of the signals

of the  $M - 1$  users in a cluster, say  $n$ th cluster, to be appeared in other  $N - 1$  subspaces. Therefore, the signals of the  $M - 1$  user in a cluster can lead to interference on the signals of the users located in  $N - 1$  clusters. Consequently, the sum-rate reduces. In the rest of the paper, we will analyze the rate reduction.

#### IV. THE SUM-RATE EVALUATION FOR HB-NOMA

As mentioned, the misalignment between the effective channel of the first user and the other users in each cluster causes the interference, as a result, the achievable rate is degraded. In this section, we focus on studying the achievable rate of  $U_{n,m}$  in two cases. In the first case, it is assumed that there is a perfect alignment between the effective channels of the users of each cluster. In other words, there is a perfect correlation between the effective channels of the users in a cluster. In the second case, it is assumed that there is a misalignment between the effective channels of the first user and the other users. In this case, the correlation is imperfect. In order to distinguish the perfect effective channel from the imperfect

---

##### Algorithm 1 The Sum-Rate Maximization

---

**Input:**  $\mathbf{H}_{n,m}$  for  $n = 1, 2, \dots, N$  and  $m = 1, 2, \dots, M$

**Output:**  $\mathbf{F}_{\text{RF}}$ ,  $\mathbf{w}_{n,m}$ ,  $\mathbf{F}_{\text{BB}}$ , and  $P_{n,m}$

**Step 1:** Designing RF precoder and combiner

For  $U_{n,m}$

The BS and the user select  $\mathbf{w}_{n,m}$  and  $\mathbf{f}_{\text{RF}}^{n,m}$  to solve

$$\underset{\mathbf{w}_{n,m}, \mathbf{f}_{\text{RF}}^{n,m}}{\text{maximize}} \quad |\mathbf{w}_{n,m}^\dagger \mathbf{H}_{n,m} \mathbf{f}_{\text{RF}}^{n,m}| \quad \text{subject to (9a) and (9c).}$$

The user sets  $\mathbf{w}_{n,m} = \mathbf{a}_U(\vartheta_{n,m})$ .

The BS sorts the users based on the channel gain and sets

$$\mathbf{F}_{\text{RF}} = \left[ \mathbf{f}_{\text{RF}}^{1,1}, \mathbf{f}_{\text{RF}}^{2,1}, \dots, \mathbf{f}_{\text{RF}}^{N,1} \right].$$

**Step 2:** Designing digital precoder

For  $U_{n,m}$

The user feeds the effective channel  $\bar{\mathbf{h}}_{n,m}$  back to the BS where

$$\bar{\mathbf{h}}_{n,m}^\dagger = \mathbf{w}_{n,m}^\dagger \mathbf{H}_{n,m} \mathbf{F}_{\text{RF}}.$$

The BS designs the digital to minimize

$$\underset{\{\mathbf{f}_{\text{BB}}^\ell\}_{\ell \neq n}}{\text{minimize}} \quad |I_{\text{inter}}^{n,m}| \quad \text{subject to (9b).}$$

The optimal solution is obtained as  $\mathbf{F}_{\text{BB}} = \bar{\mathbf{H}}^\dagger (\bar{\mathbf{H}} \bar{\mathbf{H}}^\dagger)^{-1} \Lambda$  where  $\bar{\mathbf{H}} = [\bar{\mathbf{h}}_{1,1}, \bar{\mathbf{h}}_{2,1}, \dots, \bar{\mathbf{h}}_{N,1}]$ .

**Step 3:** Computing the power for each user

The BS resorts the users

$$\|\bar{\mathbf{h}}_{n,1}\| \geq \|\bar{\mathbf{h}}_{n,2}\| \geq \dots \geq \|\bar{\mathbf{h}}_{n,M}\|, \quad \text{for } n = 1, 2, \dots, N.$$

The BS sets a fixed power for every user in the  $n$ th cluster  $\sum_{m=1}^M P_{n,m} = P_c$  regarding  $P_c = \frac{P}{N}$ .

---

effective channel, hereafter, we denote  $\bar{\mathbf{h}}_{n,m}$  as the perfect effective channel and  $\tilde{\mathbf{h}}_{n,m}$  as the imperfect effective channel. Also,  $\bar{R}_{n,m}$  and  $\tilde{R}_{n,m}$  denote the rate of  $\mathbf{U}_{n,m}$  with the perfect and imperfect effective channels, respectively.

### A. Perfect Correlation

By perfect correlation we mean that  $\mathbf{a}_{\text{BS}}(\varphi_{n,m})$  is the same for all users in the  $n$ th cluster, i.e.,  $\mathbf{a}_{\text{BS}}(\varphi_{n,1}) = \mathbf{a}_{\text{BS}}(\varphi_{n,2}) = \dots = \mathbf{a}_{\text{BS}}(\varphi_{n,M})$  for  $n = 1, 2, \dots, N$ . That is, the RF precoder vector is the same for all users in each cluster. Although, this assumption is ideal and never happens in practical scenarios, the derived lower bound characterizes insightful results on the sum-rate of HB-NOMA.

**Theorem 1.** With perfect correlation, a lower bound on the achievable rate of  $\mathbf{U}_{n,m}$  is given by

$$\bar{R}_{n,m} \geq \log_2 \left( 1 + \frac{P_{n,m} N_{\text{BS}} N_{\text{U}} |\beta_{n,m}|^2}{\sum_{k=1}^{m-1} P_{n,k} N_{\text{BS}} N_{\text{U}} |\beta_{n,m}|^2 + \eta_n} \right), \quad (25)$$

where  $\eta_n = \frac{1}{4} \left( \frac{\kappa_{\max}(\mathbf{F})}{\kappa_{\min}(\mathbf{F})} + \frac{\kappa_{\min}(\mathbf{F})}{\kappa_{\max}(\mathbf{F})} + 2 \right)$ , and  $\mathbf{F} = \mathbf{F}_{\text{RF}}^\dagger \mathbf{F}_{\text{RF}}$ .

*Proof.* Given the perfect correlation assumption and (18), the effective channel vector for  $\mathbf{U}_{n,m}$  becomes

$$\begin{aligned} \bar{\mathbf{h}}_{n,m}^\dagger &= \sqrt{N_{\text{BS}} N_{\text{U}}} \beta_{n,m} \mathbf{a}_{\text{BS}}^\dagger(\varphi_{n,m}) \mathbf{F}_{\text{RF}} \\ &= \beta_{n,m} \beta_{n,1}^{-1} \bar{\mathbf{h}}_{n,1}^\dagger. \end{aligned} \quad (26)$$

On the other hand, we have

$$\bar{\mathbf{h}}_{n,1}^\dagger \mathbf{f}_{\text{BB}}^\ell = \begin{cases} \mathbf{\Lambda}_{n,n}, & \text{for } n, \ell = 1, 2, \dots, N, \\ 0, & \text{for } \ell \neq n. \end{cases} \quad (27)$$

Therefore, using (26) and (27) the numerator in (9) becomes

$$P_{n,m} |\beta_{n,m}|^2 |\beta_{n,1}|^{-2} \mathbf{\Lambda}_{n,n}^2. \quad (28)$$

Also, the intra-cluster interference in (10) becomes

$$I_{\text{intra}}^{n,m} = \sum_{k=1}^{m-1} P_{n,k} |\beta_{n,m}|^2 |\beta_{n,1}|^{-2} \mathbf{\Lambda}_{n,n}, \quad (29)$$

and the inter-cluster interference term becomes zero, i.e.,

$$I_{\text{inter}}^{n,m} = 0. \quad (30)$$

Now, substituting (28), (29), and (30) in (9) gives

$$\begin{aligned} \bar{R}_{n,m} &= \log_2 \left( 1 + \frac{P_{n,m} |\beta_{n,m}|^2 |\beta_{n,1}|^{-2} \Lambda_{n,n}^2}{\sum_{k=1}^{m-1} P_{n,k} |\beta_{n,m}|^2 |\beta_{n,1}|^{-2} \Lambda_{n,n}^2 + 1} \right) \\ &\stackrel{(a)}{=} \log_2 \left( 1 + \frac{P_{n,m} N_{\text{BS}} N_{\text{U}} |\beta_{n,m}|^2}{\sum_{k=1}^{m-1} P_{n,k} N_{\text{BS}} N_{\text{U}} |\beta_{n,m}|^2 + (\mathbf{F}^{-1})_{n,n}} \right) \\ &\stackrel{(b)}{\geq} \log_2 \left( 1 + \frac{P_{n,m} N_{\text{BS}} N_{\text{U}} |\beta_{n,m}|^2}{\sum_{k=1}^{m-1} P_{n,k} N_{\text{BS}} N_{\text{U}} |\beta_{n,m}|^2 + \eta_n} \right), \end{aligned} \quad (31)$$

where  $\eta_n$  is defined in (25). (a) follows by plugging (22) into the expression in the first line of (31) and using simple manipulations, and (b) follows from the Kantorovich inequality [35] and the proposition below.

**Proposition 1.** [12, Lemma 3] The upper bound for the  $n$ th diagonal element of  $\mathbf{F}^{-1}$ , i.e.,  $(\mathbf{F}^{-1})_{n,n}$ , is obtained as

$$(\mathbf{F}^{-1})_{n,n} \leq \frac{1}{4\mathbf{F}_{n,n}} \left( \frac{\kappa_{\max}(\mathbf{F})}{\kappa_{\min}(\mathbf{F})} + \frac{\kappa_{\min}(\mathbf{F})}{\kappa_{\max}(\mathbf{F})} + 2 \right), \quad (32)$$

where  $\kappa_{\max}(\mathbf{F})$  and  $\kappa_{\min}(\mathbf{F})$  are the largest and smallest eigenvalues of  $\mathbf{F}$ , respectively.

Now, noting that  $\mathbf{F}_{n,n} = 1$  for  $n = 1, 2, \dots, N$  and substituting the upper bound in (32) into the second line of (31) gives the inequality (b).  $\square$

Theorem 1 indicates that when the correlation between the users in each cluster is perfect, still two terms degrade the sum-rate performance of every HB-NOMA user. The first term  $\sum_{k=1}^{m-1} P_{n,k} N_{\text{BS}} N_{\text{U}} |\beta_{n,m}|^2$  is due to using NOMA scheme which leads to inevitable intra-cluster interference. The second term  $\eta_n$  is due to realizing the beamforming with digital and analog components, i.e., hybrid beamforming. It is worth mentioning that in the fully-digital beamforming the first term exists but the second term is always one. Therefore, even under ideal condition the hybrid beamforming intrinsically imposes some loss (due to the interference) on the sum-rate. However, when  $N_{\text{BS}}$  approaches to infinity the  $\eta_n$  becomes close to one [12].

### B. Imperfect Correlation

In practical scenarios, the correlation between the users in each cluster is not perfect, i.e.,  $\mathbf{a}_{\text{BS}}(\varphi_{n,1}) \neq \mathbf{a}_{\text{BS}}(\varphi_{n,2}) \neq \dots \neq \mathbf{a}_{\text{BS}}(\varphi_{n,M})$  for  $n = 1, 2, \dots, N$ . The reason is that since  $\varphi_{n,k}$  and  $\varphi_{n,m}$  for  $k \neq m$  are independent, the probability for the event  $\varphi_{n,k} = \varphi_{n,m}$  is zero [12]. In what follows, we study the impact of imperfect correlation on the sum-rate in this subsection. Before that, we calculate the norm of the effective channel defined in (18). Defining

$$\left| \mathbf{a}_{\text{BS}}^\dagger(\varphi_{n,m}) \mathbf{a}_{\text{BS}}(\varphi_{\ell,1}) \right|^2 = K_{N_{\text{BS}}}(\varphi_{\ell,1} - \varphi_{n,m}), \quad (33)$$

where  $K_{N_{\text{BS}}}$  is Fejér kernel of order  $N_{\text{BS}}$  [36], we get

$$\|\tilde{\mathbf{h}}_{n,m}\|^2 = N_{\text{BS}} N_{\text{U}} |\beta_{n,m}|^2 \sum_{\ell=1}^N K_{N_{\text{BS}}}(\varphi_{\ell,1} - \varphi_{n,m}), \quad (34)$$

where  $\tilde{\mathbf{h}}_{n,m}$  denotes the imperfect effective channel of  $\mathbf{U}_{n,m}$ .

Now, we model the relationship between the imperfect effective channels for  $\mathbf{U}_{n,1}$  and  $\mathbf{U}_{n,m}$ . The obtained relationship, which is shown by  $\rho_{n,m}$ , plays an important role in deriving the lower bound for the achievable rate of  $\mathbf{U}_{n,m}$  for  $m > 1$ .

**Lemma 1.** Let  $\varphi_{n,m}$  be close enough to  $\varphi_{n,1}$ . The imperfect effective channel for  $\mathbf{U}_{n,m}$  with  $m > 1$  and  $\mathbf{U}_{n,1}$ , for any  $n$ , can be modeled as

$$\hat{\mathbf{h}}_{n,m} \approx \rho_{n,m} \hat{\mathbf{h}}_{n,1} + \sqrt{1 - \rho_{n,m}^2} \mathbf{g}_{n,m}, \quad (35)$$

where  $\hat{\mathbf{h}}_{n,m}$  denotes the normalized imperfect effective channel,  $\rho_{n,m} = |\hat{\mathbf{h}}_{n,m}^\dagger \hat{\mathbf{h}}_{n,1}|$ , and  $\mathbf{g}_{n,m}$  is a unit-norm vector located in the space generated by the linear combination of  $\hat{\mathbf{h}}_{\ell,1}$  for  $\ell \neq n$ .

*Proof.* See Appendix A. □

Notice that (26) shows the relationship between the perfect effective channels  $\bar{\mathbf{h}}_{n,1}$  and  $\bar{\mathbf{h}}_{n,m}$  which is simple. In contrast, the imperfect effective channels are related together through a complicated expression obtained in (35).

We next find a lower bound for the achievable rate of  $\mathbf{U}_{n,m}$  when the correlation is imperfect.

**Theorem 2.** With imperfect correlation, a lower bound on the achievable rate of  $\mathbf{U}_{n,m}$ , for  $m > 1$ , is given

by

$$\tilde{R}_{n,m} \geq \log_2 \left( 1 + \frac{P_{n,m} \rho_{n,m}^2 N_{\text{BS}} N_{\text{U}} |\beta_{n,m}|^2}{\zeta_{\text{intra}}^{n,m} + \zeta_{\text{inter}}^{n,m} + \zeta_{\text{noise}}^{n,m}} \right), \quad (36)$$

where

$$\zeta_{\text{intra}}^{n,m} = \sum_{k=1}^{m-1} P_{n,k} \rho_{n,m}^2 N_{\text{BS}} N_{\text{U}} |\beta_{n,m}|^2, \quad (37)$$

and

$$\zeta_{\text{inter}}^{n,m} = P_{\text{c}} \left( 1 - \rho_{n,m}^2 \right) N_{\text{BS}} N_{\text{U}} |\beta_{n,m}|^2 \kappa_{\max}(\mathbf{S}) \eta_n K_{N_{\text{BS}},1}, \quad (38)$$

in which  $\kappa_{\max}(\mathbf{S})$  is the maximum eigenvalue of  $\mathbf{S} = \mathbf{F}_{\text{BB}}^{-n} \mathbf{F}_{\text{BB}}^{-n\dagger}$ ,  $\mathbf{F}_{\text{BB}}^{-n}$  denotes the  $\mathbf{F}_{\text{BB}}$  after eliminating the  $n$ th column. Also, for some  $m$  we define

$$K_{N_{\text{BS}},m} = \sum_{\ell=1}^N K_{N_{\text{BS}}} (\varphi_{\ell,1} - \varphi_{n,m}), \quad (39)$$

where  $K_{N_{\text{BS}}} (\varphi_{\ell,1} - \varphi_{n,m})$  denotes the Fejér kernel in (33). Finally  $\zeta_{\text{noise}}^{n,m}$  is expressed as

$$\zeta_{\text{noise}}^{n,m} = \eta_n K_{N_{\text{BS}},1} K_{N_{\text{BS}},m}^{-1}, \quad (40)$$

where  $K_{N_{\text{BS}},m}$  is defined in (39).

*Proof.* See Appendix B. □

Since for  $U_{n,1}$  the correlation factor  $\rho_{n,1}$  is one, we have  $\bar{\mathbf{h}}_{n,1} = \tilde{\mathbf{h}}_{n,1}$ . Thus, Theorem 1 is still valid for these users.

Theorem 2 states that the achievable rate of each user depends on the correlation between the first and the intended user, and a weak correlation reduces the power of the effective channel of that user. Intra-cluster and inter-cluster power allocation are other parameters that affect the achievable rate as seen in (37) and (38). Further, (38) shows that the maximum eigenvalue of the baseband precoder is important in maximizing the achievable rate. To clarify this, we refer to (21). The effective matrix should be selected in a way that the eigenvalues of the baseband precoder are as close as possible to each other. This is because if eigenvalues are far from each other, the maximum eigenvalue will be large. This increases the value of  $\zeta_{\text{inter}}^{n,m}$  which causes less achievable rate.

Besides, the bound gives a useful insight on the clustering the users. That is, the relation between the AoD  $\varphi_{n,m}$  and the correlation factor  $\rho_{n,m}$  is nonlinear. On the other hand,  $\varphi_{n,m}$  does not explicitly appears

in the rate expression whereas  $\rho_{n,m}$  does. As a result, the clustering can be done through  $\rho_{n,m}$ s as a design criterion. That is,  $\rho_{n,m} \rightarrow 0$

When the number of antennas at the BS increases ( $N_{\text{BS}} \rightarrow \infty$ ), the lower bound in Theorem 2 can be further simplified, and we have the following lemma.

**Lemma 2.** For a large number of antennas at the BS the lower bound on the achievable rate of  $U_{n,m}$  in Theorem 2 is approximated as

$$\begin{aligned}\tilde{R}_{n,m} &\geq \log_2 \left( 1 + \frac{P_{n,m} \rho_{n,m}^2 N_{\text{BS}} N_{\text{U}} |\beta_{n,m}|^2}{\zeta_{\text{intra}}^{n,m} + \zeta_{\text{inter}}^{n,m} + \zeta_{\text{noise}}^{n,m}} \right) \\ &\approx \log_2 \left( 1 + \frac{P_{n,m} \rho_{n,m}^2 N_{\text{BS}} N_{\text{U}} |\beta_{n,m}|^2}{\zeta_{\text{intra}}^{n,m} + \zeta_{\text{inter}}^{n,m} + \zeta'^{n,m}} \right),\end{aligned}\quad (41)$$

where

$$\zeta'^{n,m} = P_{\text{c}} \left( 1 - \rho_{n,m}^2 \right) N_{\text{BS}} N_{\text{U}} |\beta_{n,m}|^2, \quad (42)$$

and

$$\zeta'^{n,m}_{\text{noise}} = K_{N_{\text{BS}},m}^{-1}. \quad (43)$$

*Proof.* For a large values of  $N_{\text{BS}}$ , both  $\kappa_{\max}(\mathbf{S})$  and  $\eta_n$ ,  $n = 1, 2, \dots, N$  approach to one. Further, for  $\ell = n$ ,  $K_{\text{BS}}(\varphi_{\ell,1} - \varphi_{n,1})$  is approximately one whereas for  $\ell \neq n$  it is zero. Hence, we approximate  $K_{N_{\text{BS}},m}^{-1}$  as one. As a result,  $\zeta_{\text{inter}}^{n,m}$  in (38) is replaced by  $\zeta'^{n,m}_{\text{inter}}$  in (42). Also,  $\zeta_{\text{noise}}^{n,m}$  in (40) is replaced by  $\zeta'^{n,m}_{\text{inter}}$  in (43).  $\square$

One can observe that when  $\rho_{n,m}$  is close enough to one the lower bound in Lemma 2 is the same as the lower bound in Theorem 1 with large values of  $N_{\text{BS}}$ . This is because for  $\rho_{n,m} \rightarrow 1$  it gives  $\zeta'^{n,m}_{\text{inter}} \approx 0$  and  $\zeta'^{n,m}_{\text{intra}} \approx 1$ .

It should be highlighted that:

- We studied only the rate performance of HB-NOMA systems under imperfect effective channel correlation. In practical scenarios the effective channel at the transmitter is quantized or noisy. This may further affect the sum-rate of the proposed HB-NOMA system.
- In Algorithm 1 fixed intra-cluster and inter-cluster power allocation strategies are ordered. Adaptive but complex power allocation procedures for users inside each cluster can be designed through iterative algorithms [37]. In practice, each cluster poses different inter-cluster interference. Therefore, Algorithm 1 will be suboptimum in term of inter-cluster power allocation. A useful inter-cluster

power allocation regarding the interference caused by each cluster is given in [38].

- The derived bound in Theorem 2 shows the achievable rate extremely depends on the correlation factor. That is to say, a low correlation can cause substantial rate reduction. Thus, in user scheduling for HB-NOMA, both large-scale gain and correlation factor should be regarded.

## V. RATE LOSS DUE TO IMPERFECT CORRELATION

Here, we investigate the achievable rate gap between the perfect correlation and the imperfect correlation. As mentioned in Section IV, under the imperfect correlation, the user cannot have a data-rate equal to the perfect correlation. The following theorem helps better understand this gap.

**Theorem 3.** The rate loss of  $U_{n,m}$  for the imperfect correlation is bounded as

$$\Delta R_{n,m} = \bar{R}_{n,m} - \tilde{R}_{n,m} \leq \log_2 \left( 1 + \frac{P_c (1 - \rho_{n,m}^2) \kappa_{\max}(\mathbf{S})}{\rho_{n,m}^2 \sum_{k=1}^{m-1} P_{n,k}} \right). \quad (44)$$

*Proof.* See Appendix C. □

A close look at in (44) indicates that under the fixed power allocation, the correlation factor  $\rho_{n,m}$  has a significant effect on the rate loss. That is, a poor correlation, i.e, small  $\rho_{n,m}$ , leads to a remarkable rate loss as it increases the numerator and at the same time decreases the denominator. Besides, a larger  $\kappa_{\max}(\mathbf{S})$  causes a bigger gap in the data-rate loss. This happens when the imperfect effective channel vector of  $U_{n,m}$ ,  $\tilde{\mathbf{h}}_{n,m}$ , and the matrix  $\mathbf{F}_{\text{BB}}^{-n}$  are not orthogonal. In this case a small angle between  $\tilde{\mathbf{h}}_{n,m}$  and one of the vectors in  $\mathbf{F}_{\text{BB}}^{-n}$  results in a big eigenvalue. This event is somehow related to  $\rho_{n,m}$ . Particularly, when  $\rho_{n,m}$  decreases, the vector  $\tilde{\mathbf{h}}_{n,m}$  gets far from the space that the vector  $\tilde{\mathbf{h}}_{n,1}$  belongs to. Meanwhile,  $\tilde{\mathbf{h}}_{n,m}$  approaches to one of the vectors in  $\mathbf{F}_{\text{BB}}^{-n}$  which means  $\kappa_{\max}(\mathbf{S})$  becomes larger.

## VI. NUMERICAL RESULTS

In this section, we discuss the numerical simulations for achievable rate of  $U_{n,m}$  and sum-rate of the HB-NOMA system in Fig. 1 under both perfect and imperfect correlation assumptions. In Section VI-A we assume  $N_U = 4$  and in Section VI-B  $N_U = 8$ . The users in each cluster have different levels of the effective channel gain, and the closest user to the BS has the highest gain. The gain levels are identical for all clusters. Also, there is a single path channel from the BS to each user and full CSI is available

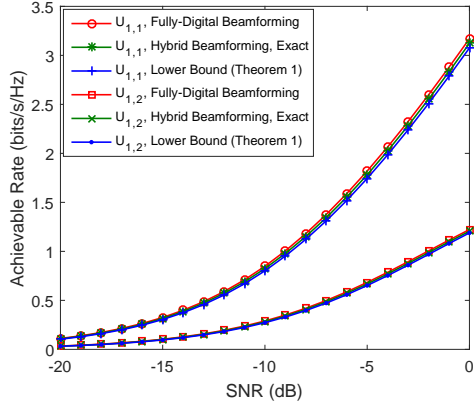


Fig. 2: The achievable rate versus SNR for the perfect correlation between  $U_{1,1}$  and  $U_{1,2}$ .

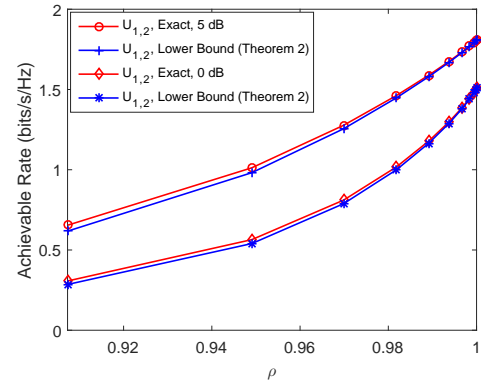


Fig. 3: Achievable rate versus correlation factor  $\rho$  between  $U_{1,1}$  and  $U_{1,2}$  for SNR equal to 5 and 0 dB and  $50^\circ \leq \varphi \leq 60^\circ$ .

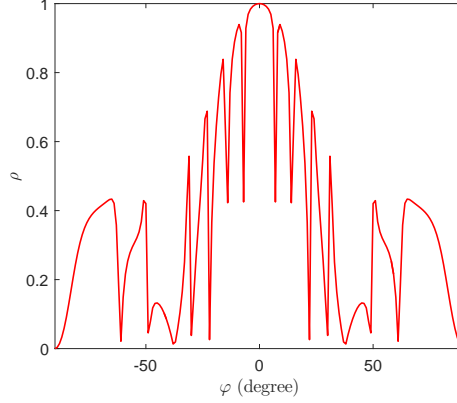


Fig. 4: Relationship between the correlation and AoD for  $U_{1,2}$  when there are three clusters. The AoDs for  $U_{n,1}$  for  $n = 1, 2$ , and 3 are assumed to be respectively  $0^\circ$ ,  $-40^\circ$ , and  $40^\circ$ .

at the BS. The elevation AoAs/AoDs have a uniform distribution in  $[-\frac{\pi}{2}, \frac{\pi}{2}]$ . The proposed algorithm in Section III-B is used to maximize the rate. Finally, we have  $P_c = P/N$ .

#### A. The Achievable Rate of $U_{n,m}$

In this section,  $N_{\text{BS}}$  and  $N_{\text{U}}$  are set to 16 and 4, respectively. In first two figures,  $M$  and  $N$  are two. The allocated power for the close user is  $1/4P_c$  and for the far user is  $3/4P_c$ . Finally, the large-scale fading, i.e.,  $d^{-\gamma}$ , is assumed 0 dB for  $U_{1,1}$  and  $U_{2,1}$  and -10 dB for  $U_{1,2}$  and  $U_{2,2}$ .

Figure 2 illustrates the achievable rate of  $U_{1,1}$  and  $U_{1,2}$  for the hybrid beamforming with the perfect correlation. By increasing the SNR both users achieve higher rates. Simulation result shows that hybrid beamforming can achieve a rate close to the fully-digital beamforming. The small gap between the two curves is due to using RF precoders that causes a residual interference. It is worth noting that in both

beamforming methods the inter-cluster interference is zero and intra-cluster interference terms are identical. The figure shows that the derived lower bound in Theorem 1 is tight.

Figure 3 evaluates the effect of the imperfect correlation on the achievable rate of  $U_{1,2}$ . It is assumed that SNR equals to 0 and 5 dB. It can be seen that a poor correlation significantly degrades the rate. For example,  $\rho = 0.92$  decreases the rate about 1 bits/s/Hz compare to  $\rho = 1$ . By increasing the correlation factor the achievable rate increases. This is because by increasing  $\rho$  inter-cluster interference, i.e.,  $\zeta_{\text{inter}}^{n,m}$ , decreases and the effective channel of the user approaches to  $U_{1,1}$  which leads to a higher value for  $K_{N_{\text{BS}}}$  in Theorem 2. Also, the figure shows that the derived lower bound in Theorem 2 is very close to the simulation value.

In Fig. 4, we investigate the relationship between the correlation ( $\rho$ ) and AoD ( $\varphi$ ) for  $-90^\circ \leq \varphi \leq 90^\circ$  for three clusters and two users. For each  $U_{n,1}$  for  $n = 1, 2$ , and 3 AoD is respectively given as  $0^\circ$ ,  $-40^\circ$ , and  $40^\circ$ . As shown the correlation between  $U_{1,1}$  and  $U_{1,2}$  around  $0^\circ$  is 1. It also shows that when AoD of  $U_{1,2}$  is in range  $[-4^\circ, 4^\circ]$  the correlation remains greater than 0.95. The lowest correlation happens around  $-40^\circ$  and  $40^\circ$  which are the AoDs of  $U_{2,1}$  and  $U_{3,1}$ . This means an efficient baseband precoder and user clustering can eliminate the interference from other clusters.

### B. The Sum-Rate

The achievable sum-rate versus  $N_{\text{BS}}$  for two values of  $P$  is plotted in Fig. 5. We set  $M = 4$  and  $N = 6$ . The AoDs of  $U_{n,1}$  for  $n = 1, 2, \dots, 6$  are given respectively by  $\{10^\circ, 20^\circ, 30^\circ, 40^\circ, 60^\circ, 80^\circ\}$ . The channel gains  $d_{n,m}^{-\nu}$  are  $\{0, -10, -20, -30\}$  dB and the allocated power are respectively  $\{0.1P_c, 0.2P_c, 0.3P_c, 0.4P_c\}$ . It is seen that by increasing number of the antennas the sum-rate of the hybrid beamforming approaches to that of the fully-digital beamforming. Also, the derived lower bound is tight.

In Fig. 6 the sum-rate of the imperfect hybrid beamforming versus  $N_{\text{BS}}$  for two values of the correlation factor has been demonstrated. Let  $M = 4$  and  $N = 3$ . The AoDs of  $U_{n,1}$  for  $n = 1, 2$ , and 3 are given respectively by  $\{10^\circ, 40^\circ, 70^\circ\}$ . The same channel gain levels and powers have been assumed as mentioned in Fig. 5. The correlation between  $U_{n,m}$  for  $m = 2, 3$ , and 4 and  $U_{n,1}$  for  $n = 1, 2$ , and 3 is set  $\rho = 0.6$  and 0.9. As  $N_{\text{BS}}$  grows up the sum-rate increases for both values of  $\rho$ . Also, at large values of  $N_{\text{BS}}$  the sum-rate for  $\rho = 0.6$  nears to that of  $\rho = 0.9$ . As can be seen from the figure, the lower bound is similar to the exact sum-rate.

Figure 7 illustrates the sum-rate of the HB-NOMA for  $N = 4$  and  $M = 2, 3$ , and 4. For this simulation, we assume that the AoDs of  $U_{n,1}$  for  $n = 1, 2, 3$ , and 4 are  $\{10^\circ, 30^\circ, 40^\circ, 60^\circ\}$ . Also, for  $M = 2$  the channel

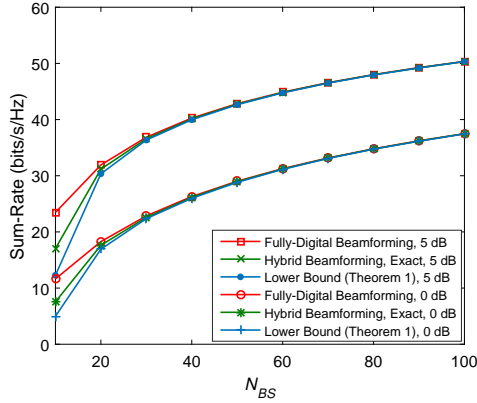


Fig. 5: The sum-rate versus  $N_{BS}$  for  $M = 4$  and  $N = 6$  with  $P = 0$  and 5 dB. The performance is depicted for fully-digital beamforming, hybrid beamforming with perfect correlation and the upper bound derived in Theorem 1.

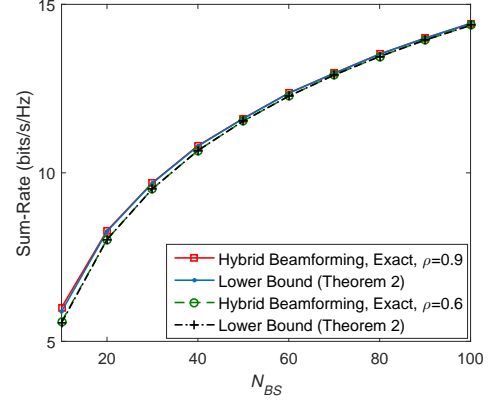


Fig. 6: The sum-rate versus  $N_{BS}$  for  $M = 4$  and  $N = 3$  with  $P = 0$  dB. The simulation has been done for the hybrid beamforming and the derived lower bound in Theorem 2.

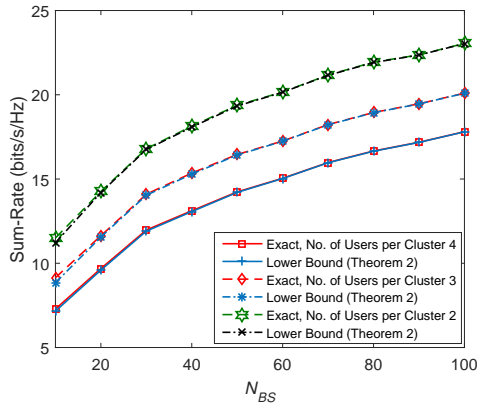


Fig. 7: The sum-rate versus  $N_{BS}$  for  $N = 4$  and  $M = 2, 3$ , and 4.

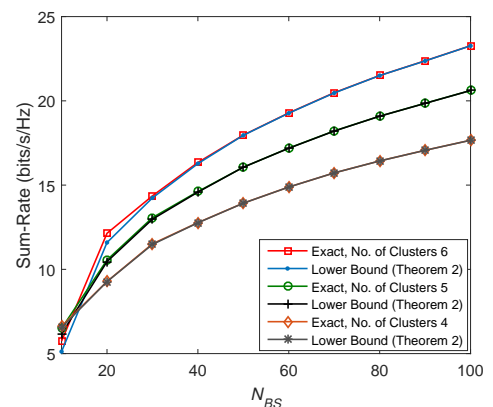


Fig. 8: The sum-rate versus number of the transmit antenna array for the imperfect HB-NOMA with  $M = 4$  and  $N = 4, 5$ , and 6. The total power is limited to 0 dB and the correlation factor is 0.8.

gains are  $\{0, -10\}$  dB with the allocated power  $\{0.25P_c, 0.75P_c\}$ , respectively. For  $M = 3$  the channel gains are  $\{0, -10, -20\}$  dB with the allocated power  $\{0.15P_c, 0.35P_c, 0.5P_c\}$ , respectively. Finally, for  $M = 4$  the channel gains are considered to be  $\{0, -10, -20, -30\}$  and the allocated power corresponding to each user is respectively  $\{0.1P_c, 0.2P_c, 0.3P_c, 0.4P_c\}$ . The total power budget is limited to 0 dB and the correlation factor is 0.9. While the sum-rate goes up by increasing  $N_{BS}$  for all curves, it decreases as the number of weak users increases in each cluster. This behavior can be justified as follows. Although NOMA simultaneously serves a huge number of users, by increasing the number of weak users the sum-rate decreases. Our simulation proves this trade-off for the proposed HB-NOMA. The lower bound found in Theorem 2 is perfectly fitted to the exact the sum-rate especially for large values of  $N_{BS}$ .

In Fig. 8 the sum-rate of the imperfect HB-NOMA is plotted for  $M = 4$  and  $N = 4, 5$ , and 6. The

channel gains and users' power are the same as those in Fig. 5. For  $N = 4, 5$ , and  $6$  the AoDs are respectively  $\{10^\circ, 30^\circ, 40^\circ, 70^\circ\}$ ,  $\{10^\circ, 30^\circ, 40^\circ, 60^\circ, 80^\circ\}$ , and  $\{10^\circ, 20^\circ, 30^\circ, 40^\circ, 60^\circ, 80^\circ\}$ . We also have  $P = 0$  dB and  $\rho = 0.8$ . Simulation result indicates that for  $N_{\text{BS}}$  fewer than about 14, by increasing the size of clusters the sum-rate decreases. Whereas, for  $N_{\text{BS}}$  larger than 14 a higher number of clusters leads to achieving a bigger sum-rate. This phenomenon points out an important issue in HB-NOMA systems that the correlation plays a significant role in imperfect HB-NOMA systems. When  $N_{\text{BS}}$  is small, due to the imperfect correlation the inter-cluster interference is severe. Consequently, adding more cluster causes intensive inter-cluster interference. In contrast, as  $N_{\text{BS}}$  increases the impact of the correlation reduces and as a result the inter-cluster interference diminishes. This issue has been shown in Fig. 6, too. Hence, by increasing  $N_{\text{BS}}$  and number of the clusters the sum-rate increases.

## VII. CONCLUSION

A hybrid beamforming-based NOMA has been designed for the downlink of a single-cell mmWave communication system. To study the achievable rate of an HB-NOMA user, we first formulated an optimization problem for the sum-rate of all users in the cell and then proposed an algorithm to solve it in three steps. In order to evaluate the sum-rate, we found a lower bound for the achievable rate of each user under perfect and imperfect correlation between the effective channel of the users in each cluster. The lower bound analysis demonstrates that perfect correlation HB-NOMA achieves a sum-rate close to that with fully-digital precoder. For the imperfect correlation, the relationship between the effective channels of the first user and other users inside a cluster was modeled. The bound for the imperfect correlation shows that it is highly function of the correlation factor. Such that, a weak correlation can cause a significant reduction in the achievable rate. Further, for each user, the rate gap between the perfect correlation and imperfect correlation is bounded. Extensive numerical simulations are conducted. The simulation results verify our findings.

## APPENDIX A

### PROOF OF LEMMA 1

*Proof.* Assume that the effective channel vectors are fed back by using infinite-resolution codebooks. Also, let  $\hat{\mathbf{h}}_{n,m}$  denote the normalized effective channel vector for  $\mathbf{U}_{n,m}$ , i.e.,

$$\hat{\mathbf{h}}_{n,m} = \frac{\tilde{\mathbf{h}}_{n,m}}{\|\tilde{\mathbf{h}}_{n,m}\|}. \quad (45)$$

The angle between two complex-valued vectors  $\tilde{\mathbf{h}}_{n,m}$  and  $\tilde{\mathbf{h}}_{n,1} \in V_{\mathbb{C}}$ , denoted by  $\Phi_C$ , is obtained as [39]

$$\cos\Phi_C \equiv \rho_{n,m} e^{j\omega_{n,m}} = \hat{\tilde{\mathbf{h}}}_{n,1}^\dagger \hat{\tilde{\mathbf{h}}}_{n,m}, \quad (46)$$

where  $(\rho_{n,m} \leq 1)$  is equal to [39]

$$\rho_{n,m} = \cos\Phi_H(\hat{\tilde{\mathbf{h}}}_{n,1}, \hat{\tilde{\mathbf{h}}}_{n,m}) = \left| \hat{\tilde{\mathbf{h}}}_{n,1}^\dagger \hat{\tilde{\mathbf{h}}}_{n,m} \right|, \quad (47)$$

in which  $\Phi_H(\hat{\tilde{\mathbf{h}}}_{n,1}, \hat{\tilde{\mathbf{h}}}_{n,m})$ ,  $0 \leq \Phi_H \leq \frac{\pi}{2}$ , is called the Hermitian angle between two complex-valued vectors  $\tilde{\mathbf{h}}_{n,1}$  and  $\tilde{\mathbf{h}}_{n,m}$  and  $\omega_{n,m}$ ,  $-\pi \leq \omega_{n,m} \leq \pi$ , is called their pseudo-angle. The factor  $\rho_{n,m}$  describes the angle between two lines in the complex-valued vector space  $V_{\mathbb{C}}$  [39].

Hence, we find the angle between two lines which are given by the two vectors  $\hat{\tilde{\mathbf{h}}}_{n,1}$  and  $\hat{\tilde{\mathbf{h}}}_{n,m}$ . So, the angle  $\omega_{n,m}$  is neglected [39]. Further, (18) shows that the relationship between any effective channel  $\tilde{\mathbf{h}}_{n,m}$  and  $\varphi_{n,m}$  is highly non-linear which leads to a non-linear relationship between  $\rho_{n,m}$  and  $\varphi_{n,m}$ . Regarding (18),  $\rho_{n,m}$  can be calculated as

$$\begin{aligned} \rho_{n,m} &= \left| \hat{\tilde{\mathbf{h}}}_{n,1}^\dagger \hat{\tilde{\mathbf{h}}}_{n,m} \right| \\ &\stackrel{(a)}{=} \frac{N_{BS}N_U \left| \beta_{n,m} \beta_{n,1} \mathbf{a}_{BS}^\dagger(\varphi_{n,m}) \mathbf{F}_{RF} \mathbf{F}_{RF}^\dagger \mathbf{a}_{BS}(\varphi_{n,1}) \right|}{\|\tilde{\mathbf{h}}_{n,m}\| \|\tilde{\mathbf{h}}_{n,1}\|} \\ &\stackrel{(b)}{\leq} \frac{N_{BS}N_U \left| \beta_{n,m} \beta_{n,1} \mathbf{a}_{BS}^\dagger(\varphi_{n,m}) \mathbf{a}_{BS}(\varphi_{n,1}) \right|}{\|\tilde{\mathbf{h}}_{n,m}\| \|\tilde{\mathbf{h}}_{n,1}\|} \stackrel{(c)}{=} \frac{\sqrt{K_{N_{BS}}(\varphi_{n,1} - \varphi_{n,m})}}{\sqrt{\sum_{\ell=1}^N K_{N_{BS}}(\varphi_{\ell,1} - \varphi_{n,m})}}. \end{aligned} \quad (48)$$

To get (a), the expression in (18) is used, and, to get (b), we assume large  $N_{BS}$  which gives  $\mathbf{F}_{RF} \mathbf{F}_{RF}^\dagger = \mathbf{I}$ . The numerator in equality (b) follows from the definition of Fejér kernel in (33) and the denominator follows from (34). Eq. (48) verifies our claim that  $\rho_{n,m}$  is a non-linear function of  $\varphi_{n,m}$ . Therefore, we interest in finding the connection between the vectors  $\hat{\tilde{\mathbf{h}}}_{n,1}$  and  $\hat{\tilde{\mathbf{h}}}_{n,m}$  in the ranges that  $\rho_{n,m}$  can be simply introduced as a function of  $\varphi_{n,m}$ .

According to Fejér kernel, for  $\varphi_{n,m} = \varphi_{n,1}$ , (48) gives  $\rho_{n,m} = 1$ ; moreover, for  $\varphi_{n,m} = \varphi_{\ell,1}$ ,  $\ell \neq n$ , and  $\varphi_{\ell,1}$  far enough from  $\varphi_{n,1}$ , (48) gives  $\rho_{n,m} \approx 0$ . The reason that we assume  $\varphi_{\ell,1}$  is far enough from  $\varphi_{n,1}$  lies in the fact that, to have an efficient clustering, these angles should be selected in a way that give minimum inter-cluster interference. Further, for  $|\varphi_{n,m} - \varphi_{n,1}| < \delta$ , the value of  $\rho_{n,m}$  changes similar to a square function. To justify this, we know that, for  $\varphi_{n,m} = \varphi_{n,1}$ , the numerator in (48) has a value close to one. Meanwhile, the  $\ell$ th term,  $\ell \neq n$ , of the denominator is about zero and the term  $\ell = n$  is one.

Therefore,  $\rho_{n,m}$  is approximately one. By moving far from  $\varphi_{n,1}$ , the numerator decreases. Since the rate of reduction is a function of Fejér kernel, for  $|\varphi_{n,m} - \varphi_{n,1}| < \delta$ , we approximate the rate of reduction with a square function. It is worth mentioning that the denominator can be considered constant. Although, by moving far from  $\varphi_{n,1}$ , the value of  $N - 1$  terms in the denominator, i.e.,  $K_{N_{\text{BS}}}(\varphi_{\ell,1} - \varphi_{n,m})$  for  $\ell \neq n$ , increases, the value of dominant term  $K_{N_{\text{BS}}}(\varphi_{n,1} - \varphi_{n,m})$  decreases. Hence, it is reasonable to consider the denominator constant. Notice that the value of  $\delta$  depends on the number of antenna at the BS, such that for large number of the antennas,  $\delta$  approaches to zero. In summary, for a large  $N_{\text{BS}}$ , we have

$$|\varphi_{n,m} - \varphi_{n,1}| \rightarrow 0 \Rightarrow \begin{cases} \rho_{n,m} \rightarrow 1, \\ K_{N_{\text{BS}}}(\varphi_{n,1} - \varphi_{n,m}) \rightarrow 1, \\ K_{N_{\text{BS}}}(\varphi_{\ell,1} - \varphi_{n,m}) \rightarrow 0, \text{ for } \ell \neq n, \end{cases} \quad (49)$$

and

$$|\varphi_{n,m} - \varphi_{n,1}| \rightarrow \delta \Rightarrow \begin{cases} \rho_{n,m} \rightarrow 1 - \epsilon, \\ K_{N_{\text{BS}}}(\varphi_{n,1} - \varphi_{n,m}) \rightarrow 1 - \epsilon', \\ K_{N_{\text{BS}}}(\varphi_{\ell,1} - \varphi_{n,m}) \rightarrow \epsilon'', \text{ for } \ell \neq n, \end{cases} \quad (50)$$

where  $\epsilon$ ,  $\epsilon'$ , and  $\epsilon''$  are given between 0 and 1. Obviously, their value depends on  $\delta$ , but finding a relationship between them is very hard.

Based on the above discussion, (49) and (50), we consider that the rate of changes, when  $\rho_{n,m}$  gets far from  $\rho_{n,1}$  and closes to  $\varphi_{\ell,1}$ , has a square trend. Consequently, the vectors  $\hat{\mathbf{h}}_{n,1}$  and  $\hat{\mathbf{h}}_{n,m}$  are approximately related together through the factor  $\rho_{n,m}$  and vector  $\mathbf{g}_{n,m}$  as

$$\hat{\mathbf{h}}_{n,m} \approx \rho_{n,m} \hat{\mathbf{h}}_{n,1} + \sqrt{1 - \rho_{n,m}^2} \mathbf{g}_{n,m}, \quad (51)$$

where  $\rho_{n,m}$  is defined in (47) and  $\mathbf{g}_{n,m}$  is a unit-norm vector located in the space generated by the linear combination of  $\hat{\mathbf{h}}_{\ell,1}$  for  $\ell \neq n$ .

We emphasize that (51) is held only for  $|\varphi_{n,m} - \varphi_{n,1}| < \delta$ . For general case, it remains an open problem, however, the assumption  $|\varphi_{n,m} - \varphi_{n,1}| < \delta$  can be justified well. In practical 5G networks, the number of user is estimated more than one million per  $km^2$  [40]. Therefore, the probability that the assumption holds is very high.  $\square$

## APPENDIX B

## PROOF OF THEOREM 2

*Proof.* Using (35), we obtain the following expressions. First,

$$\begin{aligned} |\tilde{\mathbf{h}}_{n,m}^\dagger \mathbf{f}_{\text{BB}}^n|^2 &= \rho_{n,m}^2 \left\| \tilde{\mathbf{h}}_{n,m} \right\|^2 \left| \tilde{\mathbf{h}}_{n,1}^\dagger \mathbf{f}_{\text{BB}}^n \right|^2 + \left( 1 - \rho_{n,m}^2 \right) \left\| \tilde{\mathbf{h}}_{n,m} \right\|^2 \left| \mathbf{g}_{n,m}^\dagger \mathbf{f}_{\text{BB}}^n \right|^2 \\ &\stackrel{(a)}{=} \rho_{n,m}^2 \left\| \tilde{\mathbf{h}}_{n,m} \right\|^2 \left| \tilde{\mathbf{h}}_{n,1}^\dagger \mathbf{f}_{\text{BB}}^n \right|^2 \stackrel{(b)}{=} \rho_{n,m}^2 \left\| \tilde{\mathbf{h}}_{n,m} \right\|^2 \left\| \tilde{\mathbf{h}}_{n,1} \right\|^{-2} \Lambda_{n,n}^2, \end{aligned} \quad (52)$$

in which (a) follows since  $\mathbf{g}_{n,m}^\dagger \mathbf{f}_{\text{BB}}^n = 0$  and (b) follows from (27). Second,

$$|\tilde{\mathbf{h}}_{n,m}^\dagger \mathbf{f}_{\text{BB}}^\ell|^2 = \left( 1 - \rho_{n,m}^2 \right) \left\| \tilde{\mathbf{h}}_{n,m} \right\|^2 \left| \mathbf{g}_{n,m}^\dagger \mathbf{f}_{\text{BB}}^\ell \right|^2, \quad \text{for } \ell \neq n. \quad (53)$$

Next, Using (22), (27), (34), (45), and (52), (10) becomes

$$I_{\text{intra}}^{n,m} = \sum_{k=1}^{m-1} P_{n,k} \rho^2 N_{\text{BS}} N_{\text{U}} |\beta_{n,m}|^2 \left( \mathbf{F}^{-1} \right)_{n,n}^{-1} K_{N_{\text{BS}},m} K_{N_{\text{BS}},1}^{-1}, \quad (54)$$

where  $(\mathbf{F}^{-1})_{n,n}$  is defined in Proposition 1 and  $K_{N_{\text{BS}},1}$  and  $K_{N_{\text{BS}},m}$  are defined in (39). Likewise, Using (22), (27), (34), (45), and (53), (11) becomes

$$I_{\text{inter}}^{n,m} = P_{\text{c}} \left( 1 - \rho_{n,m}^2 \right) N_{\text{BS}} N_{\text{U}} |\beta_{n,m}|^2 \sum_{\ell \neq n}^N \left| \mathbf{g}_{n,m}^\dagger \mathbf{f}_{\text{BB}}^\ell \right|^2 K_{N_{\text{BS}},m}. \quad (55)$$

Further, after substituting (52), (54) and (55) into (9), we get

$$\tilde{R}_{n,m} = \log_2 \left( 1 + \frac{\Psi}{I_{\text{intra}}^{n,m} + I_{\text{inter}}^{n,m} + 1} \right) \stackrel{(a)}{\geq} \log_2 \left( 1 + \frac{\Psi}{I_{\text{intra}}^{n,m} + \varsigma_{\text{inter}}^{n,m} + 1} \right), \quad (56)$$

where

$$\Psi = P_{n,m} \rho^2 N_{\text{BS}} N_{\text{U}} |\beta_{n,m}|^2 \left( \mathbf{F}^{-1} \right)_{n,n}^{-1} K_{N_{\text{BS}},m} K_{N_{\text{BS}},1}^{-1}, \quad (57)$$

and  $\varsigma_{\text{inter}}^{n,m}$  is given by

$$\varsigma_{\text{inter}}^{n,m} = P_{\text{c}} \left( 1 - \rho_{n,m}^2 \right) N_{\text{BS}} N_{\text{U}} |\beta_{n,m}|^2 \kappa_{\max}(\mathbf{S}) K_{N_{\text{BS}},m}, \quad (58)$$

where  $\mathbf{S} = \mathbf{F}_{\text{BB}}^{-n} \mathbf{F}_{\text{BB}}^{-n\dagger}$  and  $\mathbf{F}_{\text{BB}}^{-n}$  denotes the basedband precoder after eliminating its  $n$ th column.

To get (a), we have the following lemma.

**Lemma 3.** An upper bound of  $\sum_{\ell \neq n}^N \left| \mathbf{g}_{n,m}^\dagger \mathbf{f}_{\text{BB}}^\ell \right|^2$  is the maximum eigenvalue of  $\mathbf{S}$ , i.e.,  $\kappa_{\max}(\mathbf{S})$ .

*Proof.* We rewrite  $\sum_{\ell \neq n}^N \left| \mathbf{g}_{n,m}^\dagger \mathbf{f}_{\text{BB}}^\ell \right|^2 = \left\| \mathbf{g}_{n,m}^\dagger \mathbf{F}_{\text{BB}}^{-n} \right\|^2$ . Maximizing  $\left\| \mathbf{g}_{n,m}^\dagger \mathbf{F}_{\text{BB}}^{-n} \right\|^2$  given  $\left\| \mathbf{g}_{n,m} \right\| = 1$  is similar to maximizing a beamforming vector for maximum ratio transmission systems [41], [42]. Hence, the maximum value of  $\mathbf{g}_{n,m}$  is the dominant right singular vector of  $\mathbf{F}_{\text{BB}}^{-n}$  given in (38) [41], [42]. Thus, the maximum of  $\left\| \mathbf{g}_{n,m}^\dagger \mathbf{F}_{\text{BB}}^{-n} \right\|^2$  is the maximum eigenvalue of  $\mathbf{S}$ .  $\square$

Lemma 3 indicates that  $I_{\text{inter}}^{n,m} \leq \varsigma_{\text{inter}}^{n,m}$ . After some manipulations

$$\begin{aligned} \tilde{R}_{n,m} &\geq \log_2 \left( 1 + \frac{P_{n,m} \rho^2 N_{\text{BS}} N_{\text{U}} |\beta_{n,m}|^2}{\zeta_{\text{intra}}^{n,m} + (\varsigma_{\text{inter}}^{n,m} + 1) (\mathbf{F}^{-1})_{n,n} K_{N_{\text{BS}},m}^{-1} K_{N_{\text{BS}},1}} \right) \\ &\stackrel{(a)}{\geq} \log_2 \left( 1 + \frac{P_{n,m} \rho_{n,m}^2 N_{\text{BS}} N_{\text{U}} |\beta_{n,m}|^2}{\zeta_{\text{intra}}^{n,m} + \zeta_{\text{inter}}^{n,m} + \eta_n K_{N_{\text{BS}},m}^{-1} K_{N_{\text{BS}},1}} \right), \end{aligned} \quad (59)$$

where in the first line,  $\zeta_{\text{intra}}^{n,m} = \sum_{k=1}^{m-1} P_{n,k} \rho^2 N_{\text{BS}} N_{\text{U}} |\beta_{n,m}|^2$ . To get (a), we use the inequality in Proposition 1 that completes the proof.  $\square$

## APPENDIX C

### PROOF OF THEOREM 3

*Proof.* We start from (9) to define the achievable rate of  $\mathbf{U}_{n,m}$  for the perfect correlation and the imperfect correlation, i.e.,  $\bar{R}_{n,m}$  and  $\tilde{R}_{n,m}$ , respectively. This gives

$$\begin{aligned} \Delta R_{n,m} &= \bar{R}_{n,m} - \tilde{R}_{n,m} \\ &= \log_2 \left( 1 + \frac{P_{n,m} \left| \bar{\mathbf{h}}_{n,m}^\dagger \mathbf{f}_{\text{BB}}^n \right|^2}{\sum_{k=1}^{m-1} P_{n,k} \left| \bar{\mathbf{h}}_{n,m}^\dagger \mathbf{f}_{\text{BB}}^n \right|^2 + 1} \right) - \log_2 \left( 1 + \frac{P_{n,m} \left| \tilde{\mathbf{h}}_{n,m}^\dagger \mathbf{f}_{\text{BB}}^n \right|^2}{\sum_{k=1}^{m-1} P_{n,k} \left| \tilde{\mathbf{h}}_{n,m}^\dagger \mathbf{f}_{\text{BB}}^n \right|^2 + P_c \sum_{\ell \neq n} \left| \tilde{\mathbf{h}}_{n,m}^\dagger \mathbf{f}_{\text{BB}}^\ell \right|^2 + 1} \right) \\ &= \log_2 \left( \frac{\sum_{k=1}^m P_{n,k} \left| \bar{\mathbf{h}}_{n,m}^\dagger \mathbf{f}_{\text{BB}}^n \right|^2 + 1}{\sum_{k=1}^{m-1} P_{n,k} \left| \bar{\mathbf{h}}_{n,m}^\dagger \mathbf{f}_{\text{BB}}^n \right|^2 + 1} \right) - \log_2 \left( \frac{\sum_{k=1}^m P_{n,k} \left| \tilde{\mathbf{h}}_{n,m}^\dagger \mathbf{f}_{\text{BB}}^n \right|^2 + P_c \sum_{\ell \neq n} \left| \tilde{\mathbf{h}}_{n,m}^\dagger \mathbf{f}_{\text{BB}}^\ell \right|^2 + 1}{\sum_{k=1}^{m-1} P_{n,k} \left| \tilde{\mathbf{h}}_{n,m}^\dagger \mathbf{f}_{\text{BB}}^n \right|^2 + P_c \sum_{\ell \neq n} \left| \tilde{\mathbf{h}}_{n,m}^\dagger \mathbf{f}_{\text{BB}}^\ell \right|^2 + 1} \right) \\ &\stackrel{(a)}{\leq} \log_2 \left( \frac{\sum_{k=1}^m P_{n,k} \left| \bar{\mathbf{h}}_{n,m}^\dagger \mathbf{f}_{\text{BB}}^n \right|^2 + 1}{\sum_{k=1}^m P_{n,k} \left| \tilde{\mathbf{h}}_{n,m}^\dagger \mathbf{f}_{\text{BB}}^n \right|^2 + 1} \right) - \log_2 \left( \frac{\sum_{k=1}^{m-1} P_{n,k} \left| \bar{\mathbf{h}}_{n,m}^\dagger \mathbf{f}_{\text{BB}}^n \right|^2 + 1}{\sum_{k=1}^{m-1} P_{n,k} \left| \tilde{\mathbf{h}}_{n,m}^\dagger \mathbf{f}_{\text{BB}}^n \right|^2 + P_c \sum_{\ell \neq n}^N \left| \tilde{\mathbf{h}}_{n,m}^\dagger \mathbf{f}_{\text{BB}}^\ell \right|^2 + 1} \right) \end{aligned}$$

$$\stackrel{(b)}{\leq} \log_2 \left( \frac{\|\bar{\mathbf{h}}_{n,m}\|^2 \left| \hat{\mathbf{h}}_{n,m}^\dagger \mathbf{f}_{\text{BB}}^n \right|^2}{\|\tilde{\mathbf{h}}_{n,m}\|^2 \left| \hat{\mathbf{h}}_{n,m}^\dagger \mathbf{f}_{\text{BB}}^n \right|^2} \right) - \log_2 \left( \frac{\|\bar{\mathbf{h}}_{n,m}\|^2 \sum_{k=1}^{m-1} P_{n,k} \left| \hat{\mathbf{h}}_{n,m}^\dagger \mathbf{f}_{\text{BB}}^n \right|^2 + 1}{\Upsilon} \right), \quad (60)$$

where

$$\Upsilon = \|\tilde{\mathbf{h}}_{n,m}\|^2 \sum_{k=1}^{m-1} P_{n,k} \left| \hat{\mathbf{h}}_{n,m}^\dagger \mathbf{f}_{\text{BB}}^n \right|^2 + P_c \|\tilde{\mathbf{h}}_{n,m}\|^2 \sum_{\ell \neq n}^N \left| \hat{\mathbf{h}}_{n,m}^\dagger \mathbf{f}_{\text{BB}}^\ell \right|^2 + 1.$$

To get (a) we remove positive quantity  $P_c \sum_{\ell \neq n}^N \left| \hat{\mathbf{h}}_{n,m}^\dagger \mathbf{f}_{\text{BB}}^\ell \right|^2$  from the second term. Then, we exchange the denominator of the first term with the numerator of the second one. (b) follows from the fact that for  $u > v$ , it gives  $\log\left(\frac{u}{v}\right) > \log\left(\frac{u+1}{v+1}\right)$ , and applying the normalized vector  $\tilde{\mathbf{h}}_{n,m}$  defined in (45) for both perfect and imperfect effective channel vectors.

Noting that  $\hat{\mathbf{h}}_{n,1} = \hat{\mathbf{h}}_{n,m}$  and using (52) it yields

$$\begin{aligned} \Delta R &\leq \log_2 \left( \frac{\|\bar{\mathbf{h}}_{n,m}\|^2}{\rho_{n,m}^2 \|\tilde{\mathbf{h}}_{n,m}\|^2} \right) - \log_2 \left( \sum_{k=1}^{m-1} P_{n,k} \|\bar{\mathbf{h}}_{n,m}\|^2 \left| \hat{\mathbf{h}}_{n,1}^\dagger \mathbf{f}_{\text{BB}}^n \right|^2 \right) \\ &\quad + \log_2 \left( \sum_{k=1}^{m-1} P_{n,k} \rho_{n,m}^2 \|\tilde{\mathbf{h}}_{n,m}\|^2 \left| \hat{\mathbf{h}}_{n,1}^\dagger \mathbf{f}_{\text{BB}}^n \right|^2 + P_c (1 - \rho_{n,m}^2) \sum_{\ell \neq n}^N \left| \hat{\mathbf{h}}_{n,m}^\dagger \mathbf{f}_{\text{BB}}^\ell \right|^2 + 1 \right) \\ &\stackrel{(a)}{=} -\log_2 \left( \sum_{k=1}^{m-1} P_{n,k} \rho_{n,m}^2 \left| \hat{\mathbf{h}}_{n,1}^\dagger \mathbf{f}_{\text{BB}}^n \right|^2 \right) + \log_2 \left( \sum_{k=1}^{m-1} P_{n,k} \rho_{n,m}^2 \left| \hat{\mathbf{h}}_{n,1}^\dagger \mathbf{f}_{\text{BB}}^n \right|^2 + P_c (1 - \rho_{n,m}^2) \sum_{\ell \neq n}^N \left| \hat{\mathbf{h}}_{n,m}^\dagger \mathbf{f}_{\text{BB}}^\ell \right|^2 + \|\tilde{\mathbf{h}}_{n,m}\|^{-2} \right) \\ &\stackrel{(b)}{=} \log_2 \left( 1 + \frac{P_c (1 - \rho_{n,m}^2) \sum_{\ell \neq n}^N \left| \hat{\mathbf{h}}_{n,m}^\dagger \mathbf{f}_{\text{BB}}^\ell \right|^2}{\rho_{n,m}^2 \sum_{k=1}^{m-1} P_{n,k} \left| \hat{\mathbf{h}}_{n,1}^\dagger \mathbf{f}_{\text{BB}}^n \right|^2} + \frac{\|\tilde{\mathbf{h}}_{n,m}\|^{-2}}{\rho_{n,m}^2 \sum_{k=1}^{m-1} P_{n,k} \left| \hat{\mathbf{h}}_{n,1}^\dagger \mathbf{f}_{\text{BB}}^n \right|^2} \right) \\ &\stackrel{(c)}{\leq} \log_2 \left( 1 + \frac{P_c (1 - \rho_{n,m}^2) \sum_{\ell \neq n}^N \left| \hat{\mathbf{h}}_{n,m}^\dagger \mathbf{f}_{\text{BB}}^\ell \right|^2}{\rho_{n,m}^2 \sum_{k=1}^{m-1} P_{n,k}} \right) \stackrel{(d)}{\leq} \log_2 \left( 1 + \frac{P_c (1 - \rho_{n,m}^2) \kappa_{\max}(\mathbf{S})}{\rho_{n,m}^2 \sum_{k=1}^{m-1} P_{n,k}} \right), \end{aligned} \quad (61)$$

in which (a) follows by rewriting the first term as  $\log_2(\rho_{n,m}^{-2} \|\tilde{\mathbf{h}}_{n,m}\|^2) - \log_2(\|\tilde{\mathbf{h}}_{n,m}\|^2)$ . Then, we sum up the expression  $\log_2(\rho_{n,m}^{-2} \|\tilde{\mathbf{h}}_{n,m}\|^2)$  with the second term and the expression  $-\log_2(\|\tilde{\mathbf{h}}_{n,m}\|^2)$  with the third term. To get (b), we again sum up the first term with the second term. To obtain (c), we remove the third expression which is positive. Finally, (d) is followed by Lemma 3.  $\square$

## REFERENCES

- [1] T. S. Rappaport, S. Sun, R. Mayzus, H. Zhao, Y. Azar, K. Wang, G. N. Wong, J. K. Schulz, M. Samimi, and F. Gutierrez, “Millimeter wave mobile communications for 5G cellular: It will work!” *IEEE Access*, vol. 1, pp. 335–349, 2013.
- [2] T. S. Rappaport, R. W. Heath Jr, R. C. Daniels, and J. N. Murdock, *Millimeter wave wireless communications*. Pearson Education, 2014.
- [3] A. Osseiran, F. Boccardi, V. Braun, K. Kusume, P. Marsch, M. Maternia, O. Queseth, M. Schellmann, H. Schotten, H. Taoka *et al.*, “Scenarios for 5G mobile and wireless communications: the vision of the METIS project,” *IEEE Commun. Mag.*, vol. 52, no. 5, pp. 26–35, 2014.
- [4] J. Kim and I. Lee, “802.11 WLAN: history and new enabling MIMO techniques for next generation standards,” *IEEE Commun. Mag.*, vol. 53, no. 3, pp. 134–140, 2015.
- [5] O. El Ayach, R. W. Heath, S. Abu-Surra, S. Rajagopal, and Z. Pi, “Low complexity precoding for large millimeter wave MIMO systems,” in *Proc. 2012 IEEE Int. Conf. Commun.*, pp. 3724–3729.
- [6] O. El Ayach, S. Rajagopal, S. Abu-Surra, Z. Pi, and R. W. Heath, “Spatially sparse precoding in millimeter wave mimo systems,” *IEEE Trans. Wireless Commun.*, vol. 13, no. 3, pp. 1499–1513, 2014.
- [7] J. Brady, N. Behdad, and A. M. Sayeed, “Beamspace MIMO for millimeter-wave communications: System architecture, modeling, analysis, and measurements,” *IEEE Trans. Antennas Propagat.*, vol. 61, no. 7, pp. 3814–3827, 2013.
- [8] A. M. Sayeed and N. Behdad, “Continuous aperture phased MIMO: A new architecture for optimum line-of-sight links,” in *Proc. 2011 IEEE Int. Symp. Antennas Propagation*, pp. 293–296.
- [9] M. A. Almasi, H. Mehrpouyan, V. Vakilian, N. Behdad, and H. Jafarkhani, “Reconfigurable antennas in mmWave MIMO systems,” *arXiv preprint arXiv:1710.05111*, 2017.
- [10] ———, “A new reconfigurable antenna MIMO architecture for mmWave communication,” *arXiv preprint arXiv:1803.09314*, 2018.
- [11] A. Alkhateeb, R. W. Heath, and G. Leus, “Achievable rates of multi-user millimeter wave systems with hybrid precoding,” in *Proc. 2015 IEEE Int. Conf. on Commun. Workshop*, pp. 1232–1237.
- [12] A. Alkhateeb, G. Leus, and R. W. Heath, “Limited feedback hybrid precoding for multi-user millimeter wave systems,” *IEEE Trans. Wireless Commun.*, vol. 14, no. 11, pp. 6481–6494, 2015.
- [13] M. A. Almasi, H. Mehrpouyan, D. Matolak, C. Pan, and M. Elkashlan, “Reconfigurable antenna multiple access for 5G mmWave systems,” *arXiv preprint arXiv:1803.09918*, 2018.
- [14] Y. Saito, A. Benjebbour, Y. Kishiyama, and T. Nakamura, “System-level performance evaluation of downlink non-orthogonal multiple access (NOMA),” in *Proc. 2013 IEEE Int. Symp. Pers., Indoor Mobile Radio Commun.*, pp. 611–615.
- [15] Y. Saito, Y. Kishiyama, A. Benjebbour, T. Nakamura, A. Li, and K. Higuchi, “Non-orthogonal multiple access (NOMA) for cellular future radio access,” in *Proc. 2013 IEEE Veh. Technol. Conf., Spring*, pp. 1–5.
- [16] Z. Ding, Z. Yang, P. Fan, and H. V. Poor, “On the performance of non-orthogonal multiple access in 5G systems with randomly deployed users,” *IEEE Signal Processing Lett.*, vol. 21, no. 12, pp. 1501–1505, 2014.
- [17] K. Higuchi and A. Benjebbour, “Non-orthogonal multiple access (NOMA) with successive interference cancellation for future radio access,” *IEICE Trans. Commun.*, vol. 98, no. 3, pp. 403–414, 2015.
- [18] L. Dai, B. Wang, Y. Yuan, S. Han, I. Chih-Lin, and Z. Wang, “Non-orthogonal multiple access for 5G: solutions, challenges, opportunities, and future research trends,” *IEEE Commun. Mag.*, vol. 53, no. 9, pp. 74–81, 2015.
- [19] Z. Ding, P. Fan, and H. V. Poor, “Impact of user pairing on 5G nonorthogonal multiple-access downlink transmissions,” *IEEE Trans. Veh. Technol.*, vol. 65, no. 8, pp. 6010–6023, 2016.

[20] W. Shin, M. Vaezi, B. Lee, D. J. Love, J. Lee, and H. V. Poor, “Non-orthogonal multiple access in multi-cell networks: Theory, performance, and practical challenges,” *IEEE Commun. Mag.*, vol. 55, no. 10, pp. 176–183, 2017.

[21] ——, “Coordinated beamforming for multi-cell MIMO-NOMA,” *IEEE Commun. Lett.*, vol. 21, no. 1, pp. 84–87, 2017.

[22] M. Vaezi, Z. Ding, and H. V. Poor, *Multiple Access Techniques for 5G Wireless Networks and Beyond*. Springer, 2018.

[23] D. Tse and P. Viswanath, *Fundamentals of wireless communication*. Cambridge university press, 2005.

[24] Z. Ding, P. Fan, and H. V. Poor, “Random beamforming in millimeter-wave NOMA networks,” *IEEE Access*, 2017.

[25] Z. Ding, L. Dai, R. Schober, and H. V. Poor, “NOMA meets finite resolution analog beamforming in massive MIMO and millimeter-wave networks,” *IEEE Commun. Lett.*, 2017.

[26] B. Wang, L. Dai, Z. Wang, N. Ge, and S. Zhou, “Spectrum and energy-efficient beamspace MIMO-NOMA for millimeter-wave communications using lens antenna array,” *IEEE J. Select. Areas Commun.*, vol. 35, no. 10, pp. 2370–2382, 2017.

[27] W. Hao, M. Zeng, Z. Chu, and S. Yang, “Energy-efficient power allocation in millimeter wave massive MIMO with non-orthogonal multiple access,” *IEEE Wireless Commun. Lett.*, vol. 6, no. 6, pp. 782–785, 2017.

[28] Z. Xiao, L. Zhu, J. Choi, P. Xia, and X.-G. Xia, “Joint power allocation and beamforming for non-orthogonal multiple access (NOMA) in 5G millimeter-wave communications,” *IEEE Trans. Wireless Commun.*, vol. 17, no. 5, pp. 2961–2974, 2018.

[29] W. Wu and D. Liu, “Non-orthogonal multiple access based hybrid beamforming in 5G mmWave systems,” in *Proc. 2017 IEEE Int. Symp. Pers., Indoor Mobile Radio Commun.*, pp. 1–7.

[30] M. A. Almasi and H. Mehrpouyan, “Non-orthogonal multiple access based on hybrid beamforming for mmwave systems,” *arXiv preprint arXiv:1804.05444*, 2018.

[31] N. Jindal, “Antenna combining for the MIMO downlink channel,” *IEEE Trans. Wireless Commun.*, vol. 7, no. 10, 2008.

[32] M. Trivellato, H. Huang, and F. Boccardi, “Antenna combining and codebook design for the MIMO broadcast channel with limited feedback,” in *Proc. 2007 IEEE Conf. Rec. 41st ACSSC*, pp. 302–308.

[33] Q. H. Spencer, A. L. Swindlehurst, and M. Haardt, “Zero-forcing methods for downlink spatial multiplexing in multiuser MIMO channels,” *IEEE Trans. Signal Processing*, vol. 52, no. 2, pp. 461–471, 2004.

[34] T. Yoo and A. Goldsmith, “On the optimality of multiantenna broadcast scheduling using zero-forcing beamforming,” *IEEE J. Select. Areas Commun.*, vol. 24, no. 3, pp. 528–541, 2006.

[35] L. V. Kantorovich, “Functional analysis and applied mathematics,” *Uspekhi Matematicheskikh Nauk*, vol. 3, no. 6, pp. 89–185, 1948.

[36] R. Strichartz, *The Way of Analysis*, ser. Jones and Bartlett books in mathematics. Jones and Bartlett Publishers, 2000.

[37] Q. Zhang, Q. Li, and J. Qin, “Robust beamforming for nonorthogonal multiple-access systems in miso channels,” *IEEE Trans. Veh. Technol.*, vol. 65, no. 12, pp. 10 231–10 236, 2016.

[38] X. Chen, Z. Zhang, C. Zhong, and D. W. K. Ng, “Exploiting multiple-antenna techniques for non-orthogonal multiple access,” *IEEE J. Select. Areas Commun.*, vol. 35, no. 10, pp. 2207–2220, 2017.

[39] K. Scharnhorst, “Angles in complex vector spaces,” *Acta Applicandae Mathematica*, vol. 69, no. 1, pp. 95–103, 2001.

[40] H. Zhang, Y. Dong, J. Cheng, M. J. Hossain, and V. C. Leung, “Fronthauling for 5G LTE-U ultra dense cloud small cell networks,” *IEEE Wireless Commun. Mag.*, vol. 23, no. 6, pp. 48–53, 2016.

[41] D. J. Love, R. W. Heath, and T. Strohmer, “Grassmannian beamforming for multiple-input multiple-output wireless systems,” *IEEE Trans. Inform. Theory*, vol. 49, no. 10, pp. 2735–2747, 2003.

[42] P. A. Dighe, R. K. Mallik, and S. S. Jamuar, “Analysis of transmit-receive diversity in Rayleigh fading,” *IEEE Trans. Commun.*, vol. 51, no. 4, pp. 694–703, 2003.